

國立臺灣大學牙醫專業學院臨床牙醫學研究所
博士論文



Graduate Institute of Clinical Dentistry

School of Dentistry

National Taiwan University

Doctoral Dissertation

AEG-1/LYRIC 於頭頸部鱗狀細胞癌生物功能之研究
Study of Biological Functions of AEG-1/LYRIC
in Head and Neck Squamous Cell Carcinoma

王逸平
Yi-Ping Wang

指導教授：吳漢忠教授
江俊斌教授

Advisor: Professor Han-Chung Wu
Professor Chun-Pin Chiang

中華民國103年1月
Jan 2014

國立臺灣大學博士學位論文



口試委員會審定書

AEG-1/LYRIC 於頭頸部鱗狀細胞癌中

生物功能之研究

Study of Biological Functions of AEG-1/LYRIC in
Head and Neck Squamous Cell Carcinoma

本論文係王逸平君（學號 D96422003）在國立臺灣大學臨床牙醫學研究所完成之博士學位論文，於民國一百零二年十二月十一日承下列考試委員審查通過及口試及格，特此證明

口試委員：

吳俊忠

(簽名)

(指導教授)

江俊斌

靳應臺

洪開易

陳永豐

致謝

很快地，六年半就過去了。半工半讀的酸甜苦辣，真的是自己經歷過才知道。

在這六年之中，首先要感謝的是兩位恩師—吳漢忠教授與江俊斌教授。吳老師在繁忙的研究生涯中，仍願意撥出時間空間來指導像我這樣沒啥基礎研究底子的臨床醫師，並且透過一次次的討論及進度報告時的指示，讓我逐漸培養起基礎研究的思維及能力，並使本篇研究得以完成。而江俊斌教授更是以極大的包容心讓我可以臨床工作之餘可以全力地投入高度時間及精神要求的基礎研究，並且一步步地在臨床及醫院事務方面上扶持我。兩位老師謙和跟圓融的待人處事，更是我這後生小輩的典範。

吳老師實驗室的各位同仁，也帶給我不少助力跟啟發。高中同窗又實驗全能的瑞旻、data 產出跟喝水一樣快的政緯、沉穩睿智的美英、美麗犀利的壁君、寡言可靠又實力堅強的建勳、溫婉盡責的怡巨、高帥氣質的中道、熱心仔細的詩婷、溫和堅定的剛豪、幹細胞大師的奕奕、還有實驗室小精靈育綾，都在我這漫長的博士班生涯中，提供了無數的支援及鼓勵。

更不能不提的是我這輩子的牽手—劉怡如大博士。她以一貫積極又計畫周密的態度，鞭策著我在基礎研究的大道上邁進。一般假日，甚至連我們的婚假，都可以看到我倆的身影出現在實驗室。因為有她，我有了二十四小時的實驗顧問，也有了怎麼倒都不會滿(真的嗎?)的情緒垃圾桶。是她堅定的扶持與關懷，讓我在一次又一次的挫敗中，還能舔舔傷口繼續站起來。也是她的堅忍，可以允許我放著外面白花花的銀子不賺，卻因為興趣留在醫學中心承受一切的要求，並且以她小小的身軀，一直分攤著我的負擔。而小女唯羽的誕生，更是上天給我們最大的祝福。現在回家看到她對我們露出的燦爛笑容，真的可以療癒我們在成人世界所遭遇的紛紛擾擾。願她能健康快樂的成長。

頭頸部鱗狀細胞癌在台灣實為一特殊且複雜的癌症，其逐步增加的高發生率更是有其文化、經濟跟政治的背景。遺憾的是，雖然治療方面沒有太大的進展，但防治方面卻也進步緩慢。此一癌症是少數可以與子宮頸癌一樣為可預防的癌症，但仍持續殘害我國國民健康，並造成經濟上及健保上的負擔。其後之發展，實需有關當局及一般民眾的覺醒。醫者如我，也應繼續地探討此一危害甚巨之惡性腫瘤。

最後，若我的研究可以帶來任何益處，我將其榮耀歸與我母親與早逝的父親，是他們無止盡的愛，成就了我之為人。這份體認，當我自己成為父母之後，變得更為真切。

中文摘要

背景：雖然近年來癌症治療方式有長足進步，晚期頭頸部鱗狀細胞癌之存活率依舊不佳。近年研究顯示，astrocyte elevated gene-1 (AEG-1)此一單次穿膜蛋白雖無任何已知之功能區段，但仍在多種人類癌症中高度表現並與轉移發生及較差之存活率相關。

結果：頭頸部鱗狀細胞癌中 AEG-1 之高度表現與區域淋巴結轉移及較差之五年存活率呈正相關。將頭頸部鱗狀細胞癌細胞株中之 AEG-1 敲減表現後，其細胞群落形成、移動、及入侵能力皆為下降。此外，AEG-1 敲減表現後之頭頸部鱗狀細胞癌細胞株轉植於免疫不全小鼠中所形成的腫瘤體積及肺部轉移病灶亦皆減少。我們並發現 AEG-1 可上升 NF- κ B 中 p65 次單元之磷酸化，進而調控頭頸部鱗狀細胞癌細胞表現 MMP1 酵素。同時頭頸部鱗狀細胞癌之臨床檢體 AEG-1、磷酸化 p65 及 MMP1 之表現互相呈現統計上有意義之相關性。

結論： AEG-1 於頭頸部鱗狀細胞癌中高度表現與淋巴結轉移相關，並為頭頸部鱗狀細胞癌臨床預後之負向指標。

關鍵字： Astrocyte elevated gene-1 (AEG-1)、頭頸部鱗狀細胞癌 (HNSCC)、轉移、基質金屬蛋白酶 1 (MMP1)與 p65

Abstract

Background: The survival rate of head and neck squamous cell carcinoma (HNSCC) at advanced stage is poor, despite contemporary advances in treatment modalities. Recent studies have indicated that astrocyte elevated gene-1 (AEG-1), a single transmembrane protein without any known functional domains, is overexpressed in various malignancies and is implicated in both distant metastasis and poor survival.

Results: High expression of AEG-1 in HNSCC was positively correlated with regional lymph node metastasis and a poor 5-year survival rate. Knockdown of AEG-1 in HNSCC cell lines reduced their capacity for colony formation, migration and invasion. Furthermore, decreased tumor volume and metastatic foci were observed after knockdown of AEG-1 in subcutaneous xenografts and pulmonary metastasis assays *in vivo*, respectively. We also demonstrated that AEG-1 increased phosphorylation of the p65 subunit of NF- κ B, and regulated the expression of MMP1 in HNSCC cells. Moreover, compromised phosphorylation of the p65 (RelA) subunit of NF- κ B at serine 536 was observed upon silencing of AEG-1 in HNSCC cell lines and the expression status of AEG-1, phosphorylated p65 and MMP1 are mutually correlated in clinical specimens.

Conclusion: High expression of AEG-1 is associated with lymph node metastasis and is a negative prognostic parameter for clinical outcome in HNSCC.

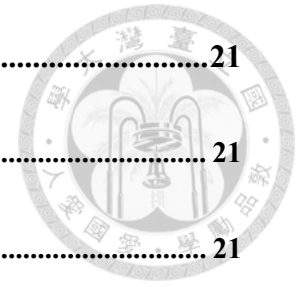
Keywords: Astrocyte elevated gene-1 (AEG-1), head and neck squamous cell carcinoma (HNSCC), metastasis, matrix metalloproteinase 1 (MMP1), p65

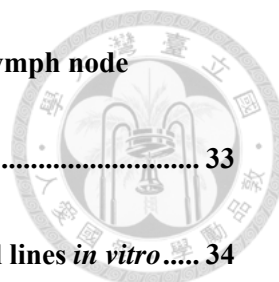
Table of content



口試委員會審定書	2
致謝.....	3
中文摘要 Table of content.....	4
Abstract.....	5
Table of content.....	6
Chapter I: Introduction.....	9
1. Head and neck squamous cell carcinoma	9
2. Astrocyte elevated gene-1	10
2.1. Initial cloning and structure.....	10
2.2 Physiological expression profile	11
2.3 Regulation of expression.....	12
2.4 Downstream signaling pathway and interacting proteins	13
2.4.1 Nuclear factor- κ B (NF- κ B).....	13
2.4.2 Phosphatidylinositol 3-kinase (PI3K/Akt).....	15
2.4.3 Staphylococcal nuclease domain-containing 1 (SND1)	17
2.5 Roles in tumor invasion/metastasis.....	18
3. Specific aims	19

Chapter II: Materials and Methods	21
1. Clinical specimen acquisition and clinicopathological staging	21
2. Immunohistochemical staining	21
3. Cell lines.....	23
4. WST-1 assays.....	24
5. Colony formation assays	24
6. Migration assays and transwell Matrigel invasion assays.....	24
7. Western blot analysis.....	25
8. <i>In vivo</i> xenograft tumor assays	26
9. <i>In vivo</i> pulmonary metastasis assay.....	27
10. Microarray analysis.....	27
11. Real-time quantitative polymerase chain reaction	28
12. Immunogold labeling and transmission electron microscopy.....	29
13. Flow cytometry.....	29
14. Luciferase assay of the MMP1 promoter region.....	30
15. Chromatin immunoprecipitation (ChIP) assay.....	31
16. Statistical analysis.....	32
Chapter III: Results.....	33





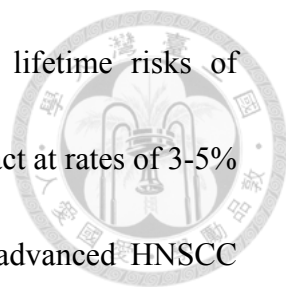
1. High AEG-1 expression in OSCC is associated with regional lymph node metastasis and unfavorable 5-year survival	33
2. AEG-1 knockdown reduced the aggressiveness of HNSCC cell lines <i>in vitro</i>	34
3. AEG-1 knockdown reduces tumor volume and pulmonary metastatic nodules of HNSCC cell lines <i>in vivo</i>	35
4. AEG-1 suppression downregulates MMP1 production	36
5. AEG-1 expression increases phosphorylation of the p65 subunit of NF- κ B and enhances p65 binding to the MMP1 promoter	37
Chapter IV: Discussion	41
Chapter V: Conclusion	51
Acknowledgement	52
References	53
Figures	64
Tables	79
Appendix	83
A. Curriculum Vita	84
B. Published article	85

Chapter I. Introduction



1. Head and neck squamous cell carcinoma

Head and neck squamous cell carcinoma (HNSCC) poses a grave threat to public health in Melanesia, South-Central Asia, and Central and Eastern Europe, with 263,900 new cases and 128,000 HNSCC related deaths reported worldwide annually [1]. This cancer usually arises within the mucosa lining the upper aerodigestive tract, with oral cavity, oropharynx, hypopharynx and larynx being the four most common affected sites. The established risk factors of HNSCC includes consumption of tobacco, alcohol and betel quids [2, 3] and the newly identified high-risk human papilloma virus (HPV) [4-6]. Regional lymph node metastasis, which is a common symptom, is present in approximately two thirds of patients with advanced stage HNSCC. Increased number of lymph nodes with metastatic lesions and the presence of extranodal spread are strong predictors for distant metastasis and poor survival of the patient [7]. Treatment plannings in HNSCC are often multi-disciplinary, including head and neck surgeons, oncologists for radiotherapy and chemotherapy, plastic surgeons and dentists. Surgery and radiotherapy are the standard treatment modalities for decades. Despite recent advances in oromaxillofacial surgery and drug therapy, such as combination treatment using either EGFR-targeting antibodies or tyrosine kinase inhibitors, there has been little improvement in the survival of patients with

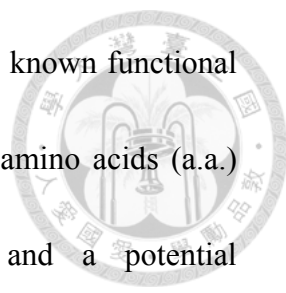


metastatic HNSCC [8-10]. Also, HNSCC patients suffer from lifetime risks of developing second primary tumors along the entire aerodigestive tract at rates of 3-5% every year [11, 12]. Furthermore, at least 50% of patients with advanced HNSCC develop locoregional metastasis or relapse within the first 2 years of treatment [13]. As such, there is an urgent need to identify new predictive parameters for lymph node metastasis and novel therapeutic targets for HNSCC.

2. Astrocyte elevated gene-1 (AEG-1)

2.1 Initial cloning and structure

AEG-1 was cloned through rapid subtraction hybridization (RaSH) for the first time in 2002 as a human immunodeficiency virus (HIV)- and tumor necrosis factor- α (TNF- α)-inducible gene in primary human fetal astrocytes [14]. Analog proteins in mouse and rat, designated as metadherin (MTDH) [15] and LYsine-RIch CEACAM1 co-isolated (LYRIC) [16], respectively, were also cloned with *in vivo* phage screening and gene trapping techniques by independent research groups. Sequence homology at nucleotide level of human AEG-1 cDNA to mouse MTDH and rat LYRIC are 90% and 89%, respectively. Sequence identity and homology at protein level of human AEG-1 to mouse MTDH were 91% and 94%, whereas to rat LYRIC were 90% and 94%, respectively. AEG-1 mRNA consists of 3611 nucleotides (poly-A tail excluded) and encodes a 582-amino acid protein with a calculated molecular weight of 64 kDa



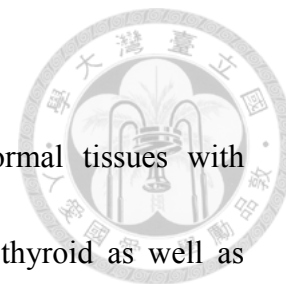
and PI of 9.33 [17]. The AEG-1 protein was reported to harbor no known functional domains except an N-terminal transmembrane domain (TMD) at amino acids (a.a.) 51-72, three nuclear localization signal (NLS) sequences and a potential ATP/GTP-binding site [15-18]. Though considered to be a single-pass transmembrane protein, the exact membrane topology of AEG-1 is still in debate. FACS analysis suggested extracellular distribution of the C-terminal [15], which supports type II topology. However, functional analysis of this molecule indicated a type I topology [16-18]. The three NLSs (NLS-1, -2, and -3 at a.a. 79-91, 432-451, and 561-580, respectively) appear to function differently in the nuclear localization. NLS-3 is essential for nuclear translocation, while an extended NLS-1 (a.a. 78-130) regulates nucleolar localization of the protein [19]. Ubiquitination at NLS-2 extension (a.a.415-486) directs the cytoplasmic localization of AEG-1 through an as yet undelineated mechanism [19]. Recent high-throughput proteomic analysis also predicted possible sites for post-translational modifications (PTM), including nine amino acid residues for phosphorylation, three for ubiquitination, and one for acetylation [20, 21]. Two phosphorylation sites (S568 and T582), two ubiquitination sites (K150 and K185) and one acetylation site (K314) are conserved between vertebrates. However, the biological significance of these PTMs on AEG-1 remains to be elucidated.

2.2 Physiological expression profile

AEG-1 mRNA expression was detected in all human normal tissues with relatively higher expression in the heart, skeletal muscle, liver, thyroid as well as adrenal glands [17]. The AEG-1 protein was reported to localized in cell membrane, cytoplasm (ER precisely), and nucleus of cells.

2.3 Regulation of expression

Treatment of TNF- α , HIV-1 gp120 glycoprotein and virions induce AEG-1 expression in astrocytes [22]. However, the mechanisms by which these inducers elevate the expression of AEG-1 in astrocytes have not been investigated. A recent study revealed tunicamycin, an ER stress-inducer, increased AEG-1 expression in neurons in a murine model for Huntington disease through unknown mechanism [23]. AEG-1 has been established as a downstream gene of the oncogene *HRAS* in various human cancers [24]. H-ras significantly induces AEG-1 through the PI3K-AKT pathway, and augments the binding of c-MYC to E-box elements in the promoter of AEG-1. Furthermore, hypoxia and glucose deprivation were shown to induce AEG-1 expression in glioblastoma cells through PI3K-AKT-associated stabilization of hypoxia induced factor-1 α (HIF-1 α) and generation of reactive oxygen species (ROS), respectively [25]. In human promonocytes, lipopolysaccharide (LPS) could increase the expression of AEG-1, which in turn to mediate LPS-induced NF- κ B activation



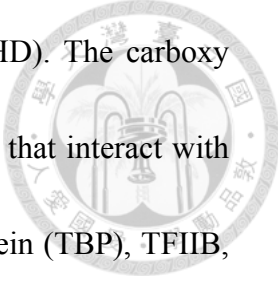
and upregulation of TNF- α and prostaglandin E2 [26].

On the other hand, AEG-1 is susceptible to miRNA suppression. There are five miRNAs that have been reported as repressor of AEG-1 expression. miR-26a decreased AEG-1 expression by targeting 3' UTR of AEG-1 RNA in clinical samples from breast cancer patient and breast cancer cell lines [27]. miR-203 and miR-22 downregulated AEG-1 expression through manipulation of AKT2 and activation of PTEN in PI3K-AKT pathway, resulting in abrogation of chemoresistance of p53-mutated colon cancer cell lines [28, 29]. However, such effect was not observed in p53 wild-type cells. A well-established tumor-suppressing miRNA, miR-375, was demonstrated to negatively regulate AEG-1 by binding to the 3' UTR of AEG-1 mRNA in clinical samples of HNSCC, hepatocellular carcinoma (HCC), breast cancer, and esophageal squamous cell carcinoma [30-34]. Finally, AEG-1 was identified as a target of miR-136 in glioma cells [35].

2.4 Downstream signaling pathway and interacting proteins

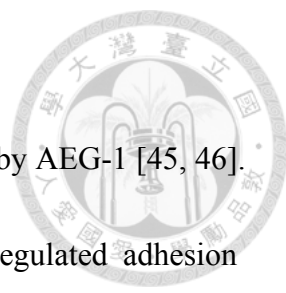
2.4.1 Nuclear factor- κ B (NF- κ B)

Although initial studies of NF- κ B subunits focused on its pivotal role in immune response, the importance of these proteins in tumor biology is appreciated now. There are five members (RELA/p65, RELB, REL/c-Rel, p50/NF- κ B1, and p52/NF- κ B2) in the mammalian NF- κ B subunit family [36] and they share a DNA-binding domain,



and a dimerization domain termed as REL homology domain (RHD). The carboxy termini of RELA, RELB, and REL contain transactivation domains that interact with basal transcription factors and cofactors such as TATA binding protein (TBP), TFIIB, E1A binding protein 300KD (EP300, also known as p300), and CREB binding protein (CBP) [37, 38]. These transcriptional coactivator proteins with histone acetyltransferase (HAT) activity are required for NF- κ B-activated transcription. Activity of NF- κ B is regulated by two major pathways, known as canonical and noncanonical pathways [39]. In resting state, NF- κ B is sequestered in the cytosol in complex with its inhibitor, I κ B. Upon stimulatory signal from surface ligand-receptor interaction or cellular stresses such as DNA damage and hypoxia, the N-terminal serine residues of I κ B are phosphorylated by the catalytic subunits of I κ B kinase (IKK) complex, IKK α and IKK β [40]. The phosphorylated I κ B is subsequently ubiquitinated and undergoes proteasomal degradation [41], resulting the nuclear translocation of NF- κ B heterodimer and its binding to the promoters of the downstream genes. Nevertheless, recent researches have revealed that the activity of NF- κ B is also determined to a great extent by numerous PTMs [42, 43]. Many genes driven by NF- κ B participate in the oncogenic progression of malignant tumors with respect to antiapoptosis (BCL2, BCLXL, BIRC5, XIAP, and c-IAPs), cell cycle control (CCND1, c-MYC, CDK2, and cyclin E), and invasion/metastasis of neoplastic cells

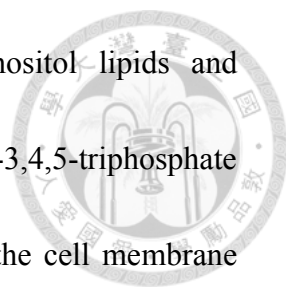
(MMP2, VCAM-1, ICAM-1, uPA, iNOS) [44].



NF- κ B is the first signaling pathway identified to be activated by AEG-1 [45, 46]. Gene array analysis showed a remarkable elevation of NF- κ B-regulated adhesion molecules (ICAM-2 and ICAM-3, selectin E, and selectin L), FOS, and JUN after ectopic expression of AEG-1 in HeLa cells [45]. Also, treatment of TNF- α in HeLa cells and malignant glioma cells triggered nuclear translocation of AEG-1 [45, 46] and increased agar cloning efficiency as well as invasion capability. Such effects were reversed when introducing an I κ B super-repressor (Ad.I κ B-mt32) [46]. Chromatin immunoprecipitation (ChIP) assay revealed that AEG-1 was physically associated with p65 and CBP on the promoter of IL-8 and inhibition of AEG-1 with siRNA impeded recruitment of CBP to the IL-8 promoter. These data suggested AEG-1 to function as a bridging protein among NF- κ B and CBP [46]. Furthermore, the region of a.a. 101-205 of AEG-1 was responsible for the docking to the p65 subunit of NF- κ B, and the proximal a.a. 1-70 was shown to be required for the binding to CBP [46, 47]. Activation of NF- κ B by AEG-1 was also observed in human prostate and liver cancer cells [48, 49].

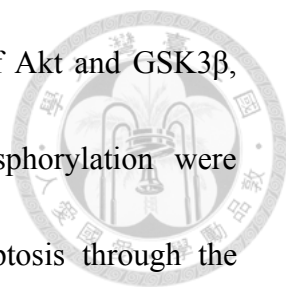
2.4.2 Phosphatidylinositol 3-kinase (PI3K/Akt)

The PI3K/Akt axis is one of the dominant regulator of a wide range of cellular functions, including proliferation, differentiation, apoptosis, motility, and metabolism



[50, 51]. Upon activation, PI3K phosphorylates membrane inositol lipids and generates the effective second messenger, phosphatidylinositol-3,4,5-triphosphate (PIP3) [52]. The Akt/PKB kinases are subsequently recruited to the cell membrane and being phosphorylated and activated by phosphoinositide-dependent kinase 1 (PDK1) and PDK2. Activated Akt translocated to cytoplasm and nucleus of cells and turn on the downstream target genes. For example, Akt phosphorylates and inactivates Bad, a proapoptotic protein of the Bcl-2 family, hence promoting cellular survival [52]. The survival-promoting capability of Akt also has been achieved through its inhibitory phosphorylation on caspase-9 [53] and modulation of transcription factors of forkhead family (FOXO) to reduce expression of Fas ligand [54]. Akt suppresses the CDK inhibitors p21 and p27 [55], and MDM2 is a phosphorylation target of Akt to facilitate G1/S phase transition in cell cycles [56]. In the meantime, Akt is negatively regulated by the phosphatase and tensin homolog deleted on chromosome 10 (PTEN) through dephosphorylation of PIP3.

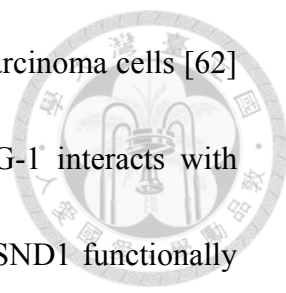
AEG-1 was initially to be demonstrated as a downstream target of PI3K/Akt pathway, since HRAS-induced AEG-1 expression was attenuated by treatment with LY294002 or PTEN overexpression [24]. The underlying mechanism was unraveled that Ha-ras increases binding of c-MYC to the E-box element in the promoter of AEG-1 through PI3K/Akt/GSK3 β cascade. It is interesting that further investigation



revealed AEG-1 overexpression also increased phosphorylation of Akt and GSK3 β , and subsequent c-MYC stabilization as well as MDM2 phosphorylation were observed [57]. Inhibition of AEG-1 was shown to induce apoptosis through the upregulation of FOXO3a in prostate cancer cells [48] and FOXO1 in breast cancer cells [58]. Activation of the PI3K/Akt pathway by AEG-1 in human hepatocellular carcinoma cells also resulted in an increased expression of multidrug resistance gene1 (MDR1) through enhanced association of MDR1 mRNA to polysomes [59]. In addition, Akt was demonstrated to be involved in AEG-1-mediated endothelial cell tube formation, upregulation of HIF-1 α , and activation of the VEGF promoter in human glioma cells [49]. Though these studies suggested AEG-1 *per se* as a potential activator of PI3K/Akt axis, the exact molecular mechanism remains to be determined.

2.4.3 Staphylococcal nuclease domain-containing 1 (SND1)

SND-1, also known as p100 coactivator or Tudor-SN, is a multifunctional protein involved in transcription, mRNA splicing, RNA interference, and mRNA stability. In the nucleus, SND-1 facilitates transcription as a coactivator and mRNA splicing by interacting with the spliceosome machinery [60]. In the cytoplasm, this protein serves as a nuclease in the RNA-induced silencing complex (RISC) to achieve RNAi-mediated gene silencing [61]. Two recent studies from independent groups identified SND1 as an associated protein of AEG-1 through yeast two-hybrid



screening with mass spectrometry confirmation in hepatocellular carcinoma cells [62] and breast cancer cells [63]. It has been demonstrated that AEG-1 interacts with SND1 in cytoplasm but not in the nucleus, and both AEG-1 and SND1 functionally facilitate RISC activity. Overexpression of AEG-1 or SND1 decreased the mRNA level of PTEN, which is a target of HCC-overexpressed miRNA-221 [62]. However, discrepancy exists regarding the interacting domain of AEG-1 to SND1, since a.a. 101-205 [62] and a.a. 364-470 [63] were both reported.

2.5 Roles in tumor invasion/metastasis

Poor prognosis of cancers at the time of diagnosis or surgery indicates a higher probability of mortality. The invasion/metastasis- promoting ability of AEG-1 has been confirmed in various cancers including glioma, prostate cancer, hepatocellular carcinoma, neuroblastoma, osteosarcoma, colorectal carcinoma (CRC), and non-small cell lung cancer (NSCLC) [48, 64-70]. MMP2 was shown to be regulated by AEG-1 in glioma and osteosarcoma [64, 66], whereas MMP9 was demonstrated as a downstream target of AEG-1 in glioma, prostate cancer and NSCLC [48, 64, 71, 72]. Brown et al. used phage display to identify AEG-1 as a receptor that mediates adhesion of murine mammary tumor 4T1 cells to lung endothelial cells and promotes lung metastasis [15]. Membranous AEG-1 has been shown to enhance adhesion of tumor cells to pulmonary microvascular endothelial cells [69]. Furthermore, a lung

homing domain (LHD) was identified at a.a. 378-440 in mouse and 381-443 in human AEG-1, respectively. Two other recent studies also revealed that AEG-1 could be involved in epithelial-mesenchymal transition in breast cancers [34, 73]. Transient ectopic expression of AEG-1 in MC7 breast cancer cells increased their migratory and invasive capability by inducing Snail, Slug, fibronectin and vimentin and suppressing E-cadherin.

Mounting evidence suggests that AEG-1 confers pleiotrophic aggressive phenotypes in malignant neoplasms, especially with respect to invasion and metastasis. Nonetheless, the definitive link between the expression of AEG-1 and its prognostic value in HNSCC patients still needs to be established with a large cohort of clinical specimen, while its underlying molecular mechanisms need to be elucidated. Since the presence of metastatic lesions has a negative impact on the prognosis and morbidity of HNSCC patients, it prompts us to investigate the biological role of AEG-1 in this disease entity.

3. Specific aims

- i. To elucidate the expression pattern of AEG-1 in clinical specimens of HNSCC and its correlation with different clinicopathological parameters.
- ii. To discover the biological functions of AEG-1 in HNSCC cell lines through *in vitro* and *in vivo* models.

- iii. To unravel the downstream effector molecules of AEG-1 and the underlying molecular regulatory mechanism.



Chapter II: Materials and Methods

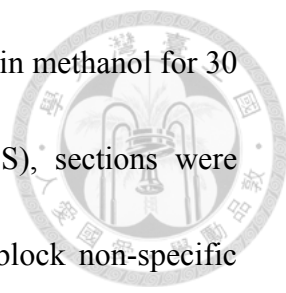


1. Clinical specimen acquisition and clinicopathological staging

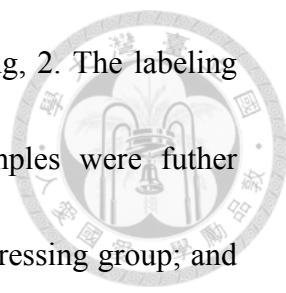
Formalin-fixed, paraffin-embedded OSCC tissue blocks were retrieved (79 men and 14 women, mean age 53.9 years, range 25-82 years) from the archive of the Department of Oral Pathology from 2000 to 2003, in accordance with ethical and institutional guidelines and with the approval of the Institutional Review Board of National Taiwan University Hospital (NTUH IRB, No 201111048RIC). Diagnosis of squamous cell carcinoma was based on histological examination of hematoxylin and eosin-stained (H&E) tissue sections by two qualified oral pathologists (YP Wang and CP Chiang). The pathological stage of each case at the time of surgery was determined according to the 7th edition of staging criteria from the American Joint Committee on Cancer. Also, specimens of oral mucosa from healthy volunteer donors with informed consent (30 cases) were collected as controls during the extractions of their impacted wisdom teeth. Tissue sections, which included both tumor and adjacent non-tumor parts for comparison purposes, were cut to 4 μ m in thickness.

2. Immunohistochemical staining

Sections were deparaffinized and rehydrated, and antigen retrieval was performed concomitantly in the Trilogy buffer system (Cell Marque, Rocklin, CA, USA) in accordance with the manufacturer's instructions. Endogenous peroxidase



activity was then blocked by immersing the sections with 3% H₂O₂ in methanol for 30 minutes (min). After washing in phosphate-buffered saline (PBS), sections were incubated with 1% bovine serum albumin (BSA) for 30 min to block non-specific binding. Sections were then incubated with the monoclonal antibody Lyric 4-7 [74] at a concentration of 1 µg/ml for one hour (hr) at room temperature (RT). For staining of phosphorylated p65 and MMP1, anti-phosphorylated p65 polyclonal antibody (sc-101753, Santa Cruz biotechnology, Dallas, TX, USA) and anti-human MMP1 antibody (clone 36665, R&D system, Minneapolis, MN, USA) were used at a dilution of 1:50 and 15 µg/ml, respectively. After being washed in PBS containing 0.1% Tween 20 (PBST_{0.1}), sections were treated with the polymer-based Super Sensitive IHC detection system (Biogenex, San Ramon, CA, USA). In brief, sections were incubated with Super Enhancer reagent for 20 min at RT and were then thoroughly rinsed three times with PBST_{0.1} for 5 min each. Sections were subsequently treated with Poly-HRP reagent for 30 min at RT. Diaminobenzidine hydrochloride (DAB) (0.02%) containing 0.03% H₂O₂ was used as a chromogen to visualize peroxidase activity. The preparations were lightly counterstained with hematoxylin, mounted with Permount (Fisher Scientific, Pittsburgh, PA, USA), and examined by light microscopy. The population index (PI) was defined as: less than 10% positive tumor cells, 0; 10-49% positive tumor cells, 1; more than 50% positive tumor cells, 2. The intensity



index (II) of the signal was designated as: none, 0; weak, 1; strong, 2. The labeling score (LS) was the product of PI and II for each case. Samples were further categorized as: LS = 0, nil-expressing group; LS = 1 or 2, low-expressing group; and LS = 4, high-expressing group. Tissue sections incubated with normal mouse IgG (NMIgG) instead of primary antibody were used as negative controls. All histopathological images were taken with an Olympus BX51 microscope and DP2-BSW image acquisition software.

3. Cell lines

OSCC cells lines HSC-3, SAS, and Ca9-22 were purchased from Japanese Collection of Research Bioresources Cell Bank and cell lines Cal 27 (OSCC) and FaDu (pharyngeal squamous cell carcinoma) were purchased from American Type Culture Collection. All cell lines were cultured in recommended media and were used in less than 6 months after resuscitation. The authenticity of SAS and FaDu cell lines was confirmed by STR profiling at Bioresource Collection and Research Center (BCRC) (Hsinchu, Taiwan). Stable AEG-1 knock-down clones of SAS and FaDu cells (SA to SE cells and FA to FE cells, respectively) were established through transfection with lentiviral vectors carrying various AEG-1-specific shRNA sequences from the National RNAi Core Facility of Academia Sinica. As controls, stable clones transfected with scrambled shRNA were generated for each cell line (SCt cells and

FCt cells, respectively). Stable clones were selected by treatment of the cells with 2 $\mu\text{g/ml}$ puromycin for 14 days. Knockdown efficiency was determined by measuring mRNA and protein by real-time quantitative polymerase chain reaction (RT-QPCR) and Western blot, respectively (Figure 3).

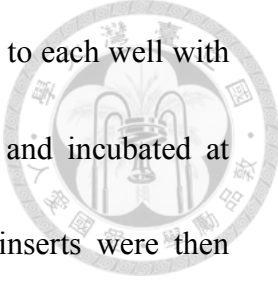
4. WST-1 assays

Cells were seeded in 96 well-plates at a concentration of 3×10^3 cells/well with matched media. One day later, 4-[3-(4-iodophenyl)-2-(4-nitrophenyl)-2H-5-tetrazolio]-1,3-benzene disulfonate (WST-1, Roche, Indianapolis, IN, USA) was added to every well at a concentration of 0.5 mg/ml, and the cells were incubated for 3 hr at 37°C. After incubation, the absorbance of the reaction products at a wavelength of 440 nm was measured, and considered as the absorbance for Day 0. The procedure was repeated each day for the next four days (Day 1 to Day 4).

5. Colony formation assays

Cells were inoculated in 6 cm dishes (1×10^3 cells/dish) and kept at 37°C for 10 days. The colonies that formed were fixed with 4% paraformaldehyde for 5 min, and then stained with 1% crystal violet for 20 min. Colonies larger than 1 mm in diameter were counted and the total number recorded.

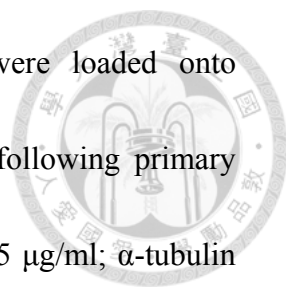
6. Migration assays and transwell Matrigel invasion assays



For the migration assay, SCt, SB, FCt and FB cells were added to each well with culture-inserts (Ibidi, Martinsried, Germany) (1×10^4 cells/well) and incubated at 37°C with 5% CO_2 . Confluence was achieved 36 hr later. The inserts were then removed, and the initial gaps were $500 \mu\text{m}$ wide. Serial photographs were taken at 4 hr intervals. For the invasion assay, Matrigel basement membrane matrix (BD Biosciences, San Jose, CA, USA) was coated to the upper side of hanging cell culture inserts (Millipore, Billerica, MA, USA) at a concentration of 2 mg/ml. Cells were seeded into the coated hanging inserts (2×10^5 cells/insert) and incubated with the corresponding culture media. The lower chamber of the invasion system was filled with serum-free culture media. The cells and Matrigel on the upper side of the inserts were removed after 24 hr. The migrated cells on the lower surface of the inserts were fixed with methanol and counted after visualization with 10 fold diluted Giemsa stain. In MMP inhibitor transwell assays, MMP inhibitor I (MMPInhI, Merck, Whitehouse Station, NJ, USA) was incorporated into corresponding culture media at a concentration of $2 \mu\text{M}$ in the hanging inserts and the diluted Matrigel. As for NF- κB inhibition assay, $5 \mu\text{M}$ MG132 was supplemented within the corresponding culture media in the hanging inserts and the diluted Matrigel for 24 hr.

7. Western blot analysis

Western blots were performed using standard protocols, as previously described



[74]. Total cell protein lysates of the indicated cell lines were loaded onto polyacrylamide gels supplemented with SDS (40 µg/lane). The following primary antibodies were used at the indicated concentrations: Lyric 4-7, 0.5 µg/ml; α -tubulin (Sigma-Aldrich Corporation, St. Louis, MO, USA), 5000-fold dilution; and MMP1 (clone 36665, R&D system, Minneapolis, MN, USA), 1 µg/ml. Antibodies against the following proteins were purchased from Cell Signaling Technology (Danvers, MA, USA) and were used at a 1000-fold dilution: NF- κ B (E498), phospho-NF- κ B p65 (Ser536) (93H1), c-Jun (60A8), phospho-c-Jun (Ser63) (54B3), phospho-c-Jun (Ser73) (#9164), pan-Akt (C67E7), phospho-Akt (Ser473) (D9E), phospho-Akt (Thr308) (C31E5), phospho-GSK-3 β (5B3), phospho-c-Raf, I κ B α (L35A5), phospho-I κ B α (serine32) (14D4), and phospho-NF- κ B p65 (Ser468) (#3039)

8. *In vivo* xenograft tumor assays

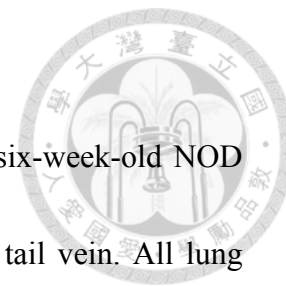
SCt, SB, FCt and FB cells were subcutaneously inoculated in pairs into the flanks of 6-week-old NOD SCID mice (1×10^6 cells/mouse, n = 6 per group). Laboratory animal husbandry and *in vivo* experiments were performed as per the guidelines of the National Laboratory Animal Center. The diameter of the resulting tumors were measured twice per week, and tumor volume was calculated as follows: large diameter \times (small diameter)² \times 0.52. Xenograft tumors were harvested at the end point of the experiment and were sent for routine tissue processing.

9. *In vivo* pulmonary metastasis assay

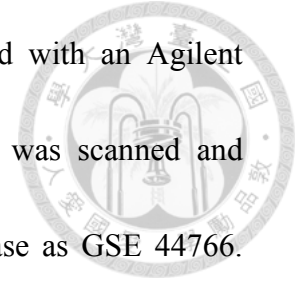
SCt, SB, FCt and FB cells were intravenously injected into six-week-old NOD SCID mice (2×10^5 cells/mouse, n = 10 per group) through the tail vein. All lung lobes were harvested twelve weeks later. Routine tissue processing was subsequently performed, and pulmonary metastatic foci were counted in sections stained with H&E.

10. Microarray analysis

Total RNAs from SCt and SB cells were extracted with 1 ml TRI reagent (Invitrogen, Carlsbad, CA, USA) and incubated for 5 min at RT. Two hundred microliters of chloroform were added to the RNA, and the mixture was shaken vigorously for 15 seconds before being incubated for 5-15 min at RT. The mixtures were then subjected to centrifugation at 12,000 g for 10-15 min at 4°C. The aqueous phase was transferred to a fresh tube and incubated with 500 μ l isopropanol for 5-10 min at RT. After centrifugation at 12,000 g for 10 min at 4°C, the supernatants were discarded and the RNA pellets washed with 1 ml 75% ethanol. The ethanol was then removed and the RNA pellets dissolved in 20 μ l H₂O. RNA extracts from SCt and SB cells were sent to the Microarray Core Facility of the Institute of Molecular Biology, Academia Sinica. Reverse transcription with aa-dUTP labeling was performed, and the associated RNA was subsequently degraded and removed. The resulting DNA



probes were coupled with Alexa/CyDye, washed and hybridized with an Agilent human V2 GX array (44Kx4). The fluorescence of the array was scanned and analyzed, and the raw data were uploaded into the GEO data base as GSE 44766.

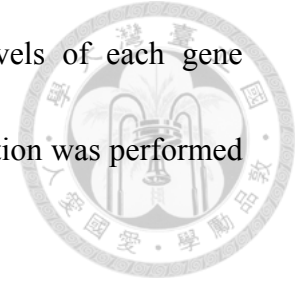


Genes with a greater than 2.5 fold change (FC) in expression were then recorded.

11. Real-time quantitative polymerase chain reaction

Total RNA was extracted from SCt, SB, FCt and FB cells as described above. Reverse transcription was performed using 4 µg aliquots of total RNA with Super-Script III RNase H-reverse transcriptase (Invitrogen, Carlsbad, CA, USA) and oligo (dT) primers (Fermentas, Glen Burnie, MD, USA), as per the manufacturer's instructions. RT-QPCR was performed using SYBR Green and the LightCycler480 II System (Roche Applied Science, Indianapolis, IN, USA). The primers used were as follows: AEG-1, GAAGAAGCAAGGTGAAGATAACT (forward) and TTGGACGGGTTTTAGAGGTATT (reverse); MMP1, CTGGAAGGGCAAGGACTCTA (forward) and CTTCCCAGCCTCTTGCTG (reverse); E-Cadherin, GGAACTATGAAAAGTGGGCTTG (forward) and AAATTGCCAGGCTCAATGAC (reverse); Snail, CTTCGGCTCCAGGAGAGTC (forward) and TTCCCACTGTCCTCATCTGAC (reverse); Slug, TGGTTGCTTCAAGGACACAT (forward) and GTTGCAGTGAGGGCAAGAA (reverse); Twist, AAGGCATCACTATGGACTTTCTCT (forward) and

GCCAGTTTGATCCCAGTATTTT (reverse). The expression levels of each gene were normalized to that of GAPDH in the same sample. Each reaction was performed in triplicate.



12. Immunogold labeling and transmission electron microscopy

SAS cells were harvested (1×10^7 cells) and sent to the Electron Microscope Core Facility of the Institute of Cellular and Organismic Biology, Academia Sinica, for sample preparation and ultrathin sectioning. The sections were then washed with Tris-buffered saline (TBS) for 15 min, and blocked with 1% BSA for 15 min. Primary antibodies against AEG-1 (or NMIgG for negative controls) was applied at a concentration of 0.5 $\mu\text{g/ml}$ for 1 hour at RT. Sections were then washed four times with TBS (5 min/wash), before being incubated with secondary anti-mouse IgG conjugated to 18 nm gold particles for 1 hour at RT. After incubation, the sections were thoroughly washed four times with TBS (5 min/wash) and five times with ddH₂O (5 min/wash). Next, the sections were treated with 5% uranyl acetate in H₂O for 10 min, and then with 0.5% lead citrate for 4 min before being completely air dried. The sections were examined with a transmission electron microscope (Hitachi H-7000).

13. Flow cytometry

SCt, SB, FCt, and FB cells were detached with 2 mM EDTA and washed with

PBS. The cells (1×10^5) were incubated with following antibodies: Lyric 4-7 or 4G2 at concentration of 0.37 $\mu\text{g/ml}$ for 1 hr at 4°C. They were then probed with PE-conjugated anti-mouse IgG (Jackson ImmunoResearch) for 30 min at 4°C. After the final wash, the cells were re-suspended with 1% FBS in PBS and analyzed by flow cytometry (BD, San Jose, CA).

14. Luciferase assay of the MMP1 promoter region

The full length promoter region of the MMP1 gene [75] was cloned from of SAS cell genomic DNA using KAPA HiFi DNA polymerase with the following primers:

CCCCTCGAGAGATGTAAGAGCTGGGAAAGGACGG (forward) and

CCCAAGCTTTCAGTGCAAGGTAAGTGATGGCTTC (reverse). To generate a

truncated fragment without the NF- κ B binding site, the following primers were used:

CCCCTCGAGCGATCTTCCATGAATACCTAACTGG (forward) and

CCCAAGCTTTCAGTGCAAGGTAAGTGATGGCTTC (reverse). The cloned full

length or truncated MMP1 promoters (nucleotides -2471 to +52) and luciferase

reporter vector pGL4 (Promega, Madison, WI, USA) were digested with Xho I and

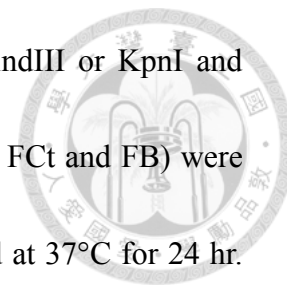
HindIII. The full length or truncated promoter sequence was then ligated into pGL4

with T4 ligase at 16°C overnight. The resulting reporter vectors were designated as P1

(-4372 to +52) and P2 (-2471 to +52). Reporter vectors P3 (containing nucleotides

-2269 to +52) and P4 (containing nucleotides -521 to +52) were generated by

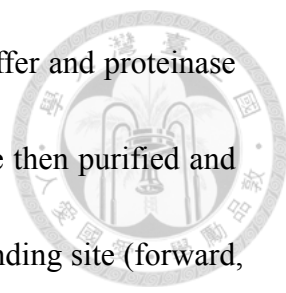
digesting the truncated MMP1 promoter either with SacI and HindIII or KpnI and HindIII, respectively, before ligating it into pGL4. Cells (SCt, SB, FCt and FB) were seeded onto 24-well plates (1×10^5 cells/well) and were incubated at 37°C for 24 hr.



The culture media was refreshed, and transfection with a reporter vector (one of P1 to P4) together with pGL4 (400 ng) and control *Renilla* vector (100 ng) was performed 30 min later, using Genejet (SignaGen laboratories, Rockville, MD) as per the manufacturer's protocol. Firefly luciferase and Renilla readouts were acquired 18 hours post-transfection using the Dual-Glo Luciferase Assay System (Promega, Madison, WI, USA) according to the manufacturer's recommendations.

15. Chromatin immunoprecipitation (ChIP) assay

ChIP assay was performed with the Magna ChIP™ G kit (Millipore, Billerica, MA, USA) in accordance with the manufacturer's protocol. In brief, 1×10^7 cells were fixed with 1% paraformaldehyde and were lysed with cell lysis buffer and nuclear lysis buffer supplemented with protease cocktail inhibitors. Lysates were sonicated to shear the crosslinked DNA to a size of 200-1000 base pairs. Equal amounts of sheared cross-linked DNA were incubated at 4°C overnight on a shaker, with protein G magnetic beads coupled to either Lyric 4-7, anti-p65 antibody (L8F6, Cell Signaling, Danvers, MA, USA), anti-CREB binding protein (CBP) antibody (D9B6, Cell Signaling, Danvers, MA, USA) or NMIgG (as a negative control). The



captured DNA-protein complexes were dissociated with elution buffer and proteinase K at 62°C for 2 hours with shaking. The free DNA fragments were then purified and quantified by RT-QPCR using primers (50 μM) flanking the p65 binding site (forward, GAGTTACAAAATTAACGGCTGA and reverse, CTGGCTGCTCTGTGAAAG). SYBR fluorescence was measured with a Lightcycler 480 II (Roche Applied Science, Indianapolis, IN, USA).

16. Statistical analysis

The associations between clinicopathological parameters and the expression status of AEG-1, phosphorylated p65, and MMP1 within clinical specimens were analyzed by Fisher's exact test. Disease-specific survival was compared between groups by Kaplan-Meier cumulative survival analysis with log-rank tests. All *in vitro* comparisons between HNSCC cells transfected with control shRNA and their experimental counterparts were performed with 3 technical replicates and 3 independent biological replicates (n = 3). Data analyses of *in vitro* experiments were performed by *t*-test. A *p*-value of less than 0.05 was considered statistically significant for all tests.

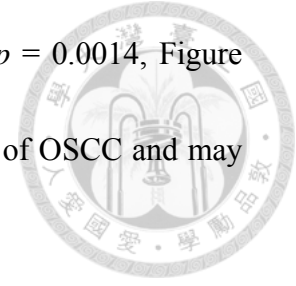
Chapter III: Results



1. High AEG-1 expression in OSCC is associated with regional lymph node metastasis and unfavorable 5-year survival

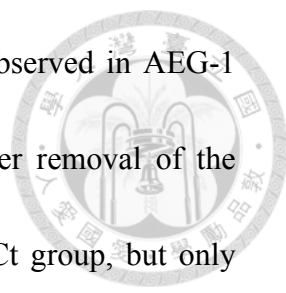
Immunohistochemical analysis of AEG-1 revealed high expression of AEG-1 in 40.86% (38 out of 93) of examined OSCC clinical specimens. AEG-1 was primarily located in the cytoplasm (the perinuclear region, in particular) of the neoplastic cells, and focal nuclear stains were also observed. In tumors with low AEG-1 expression, the majority of AEG-1-positive cells were found at the peripheral cells of the tumor nests, and not in the more-differentiated malignant cells (Figure 1A). In addition, no positive signal of AEG-1 was discerned in all 30 cases of uninflamed normal oral mucosa (Figure 2). Of the clinical parameters examined, late clinical stage ($p = 0.01$) and positive regional nodal metastasis ($p < 0.001$) were found to be significantly correlated to AEG-1 expression (Table 1). Furthermore, advanced lymph node metastasis (N2 and N3) is more common in the high AEG-1-expressing group ($p = 0.012$, Table 2). The incidence of distant metastasis was also elevated (albeit not significantly) in the high AEG-1-expressing group, as compared to that in the low and nil AEG-1-expressing groups (10.53% and 1.83%, respectively). Furthermore, a statistically significant reduction in the 5-year disease-specific survival rate was observed in the high AEG-1-expressing group as compared to that in the low and nil

AEG-1-expressing groups (36.84% versus 69.09%, log-rank test $p = 0.0014$, Figure 1B). These results imply that AEG-1 is associated with metastasis of OSCC and may serve as a negative prognostic factor for survival.



2. AEG-1 knockdown reduced the aggressiveness of HNSCC cell lines *in vitro*

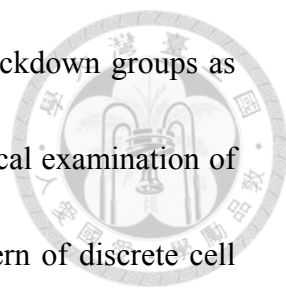
To establish an *in vitro* platform for elucidation of the biological function of AEG-1 in HNSCC cell lines, we examined the expression status of AEG-1 in several cell lines generated from HNSCC. Western blots revealed that AEG-1 was ubiquitously expressed in all HNSCC cell lines tested (Figure 1C). We subsequently generated stable clones of SAS and FaDu cells expressing AEG-1-shRNA clones and tested the knockdown efficiency and the impacts on the biological phenotypes. The clone AEG-1-shRNA-B, in which AEG-1 mRNA and protein are efficiently suppressed (SB and FB cells, respectively; Figures 3 to 5), was selected for further investigation. Although marginal inhibition of cellular proliferation was observed after knockdown of AEG-1 in SB cells, FB cells demonstrated remarkable reduction in proliferation (77.39%, $p = 0.056$ and 57.07%, $p < 0.001$ on average as compared to the corresponding control, respectively, by day 4 after seeding, Figure 4A). A dramatic reduction of colonies was also observed in both SB and FB cells, as compared to that in the relevant control (77 versus 165 colonies and 48 versus 215 colonies on average for the SAS groups and FaDu groups, respectively, Figure 4B).



Delayed wound healing and reduced Matrigel penetration were observed in AEG-1 knockdown cells (Figures 4C and D, respectively). At 12 hr after removal of the inserts, cells covered 96.9% of the visualized field area in the SCt group, but only 74.5% in the SB group (66% and 64.4% at the initial time point, respectively, Figure 4C). For the FaDu group at 12 hr, 85.9% and 78.5% of the areas were occupied by FCt and FB cells, respectively (initial, 70.8% and 70.1%, Figure 4C). The number of penetrated cells in AEG-1 knockdown cells was about 10% of the relevant control, for both SAS and FaDu cells (Figure 4D). These observations suggest that AEG-1 contributes to aggressive phenotypes of HNSCC cells, particularly with regards to their migration and invasion capacities.

3. AEG-1 knockdown reduces tumor volume and pulmonary metastatic nodules of HNSCC cell lines *in vivo*

To evaluate the biological impact of AEG-1 knockdown on HNSCC cell lines *in vivo*, subcutaneous xenografts were implanted into the flanks of NOD SCID mice. Consistent with the results acquired *in vitro*, the volume of tumors arising from AEG-1-knockdown cells was smaller than those arising from the relevant control cells at all time points examined, with the suppression effect being more evident in FaDu cell lines (394.99 versus 714.71 mm³ in the SAS group and 207.70 versus 1314.33 mm³ in the FaDu group at the end point, Figure 6A). The tumor weight at the



end-point of the experiment was also decreased in the AEG-1-knockdown groups as compared to that in the control groups (Figure 6B). Histopathological examination of harvested xenografts revealed infiltrating invasion fronts in a pattern of discrete cell nests in four out of six tumors from SCt cells and in three out of six tumors from FCt cells (Figure 6C). However, all xenografts from SB and FB cells assumed an expansile pattern of growth. Furthermore, perineural encroachment by the tumor cells was evident in two xenografts from the SCt cells. The numbers of pulmonary metastatic foci in the AEG-1-knockdown groups were also remarkably less than those of the corresponding control groups, and the size of the metastatic foci from SB cells was smaller than those observed in the SCt group (Figure 6D). These *in vivo* observations are consistent with the findings in clinical specimens and further support the hypothesis that AEG-1 is involved in the metastatic cascade of HNSCC.

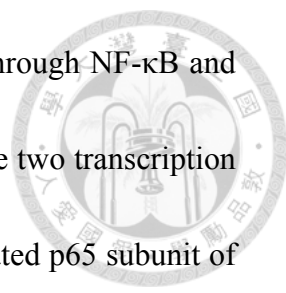
4. AEG-1 suppression downregulates MMP1 production

To determine the downstream targets of AEG-1 that contribute to invasion and metastasis pathways in HNSCC cells, we performed a microarray comparison between the gene expression profiles of SB and SCt cells. The expression level of MMP1 (matrix metalloproteinase 1) in SB cells was downregulated by approximately 3.3 fold, as compared to that in SCt cells (Figure 7A). RT-QPCR analysis also revealed a reduction in MMP1 mRNA in SB and FB cells (reduced to an average of

17.17% and 13.44% of the levels in the relevant controls, respectively, Figure 7B). In addition, AEG-1 knockdown caused a remarkable reduction of secreted MMP1 protein in the cell-conditioned culture media for both SAS and FaDu cells (Figure 7C).

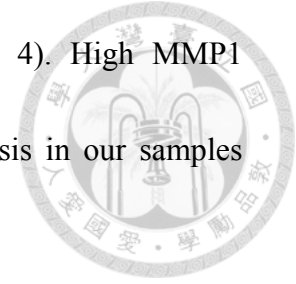
Immunohistochemical staining of MMP1 revealed a reduced positive signal in tumor xenografts and pulmonary metastatic lesions generated from AEG-1-knockdown HNSCC cells, as compared to the cytosolic and juxtacellular staining of MMP1 observed in lesions arising from control cells (Figure 7D). Also, incorporation of MMP inhibitor I (2 μ M) hampered the invasion abilities of SAS and FaDu cells in transwell assays (Figure 8). As MMPs are considered to be involved in both invasion and metastasis, MMP1 may be a downstream effector of AEG-1 in determining the aggressive phenotype of HNSCC. Since epithelial-mesenchymal transition (EMT) is also a well-known process in regards to cell motility and invasion, we investigated the expression pattern of key molecules of EMT. RT-QPCR comparison between the gene expression patterns between SCt and SB cells reveal no significant difference between E-cadherin, Snail and Slug. However, downregulation of vimentin (67% of SCt cells) and Twist (81.6% of SCt cells) was observed after knockdown of AEG-1 in SAS cells (Figure 9).

5. AEG-1 expression increases phosphorylation of the p65 subunit of NF- κ B and enhances p65 binding to the MMP1 promoter

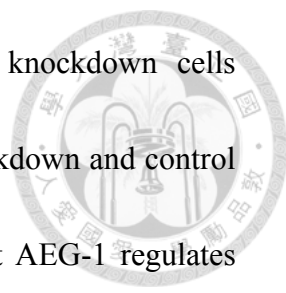


We hypothesized that AEG-1 may affect MMP1 expression through NF- κ B and AP1, since the promoter of MMP1 harbors regulation sites for these two transcription factors. Western blotting revealed that the levels of the phosphorylated p65 subunit of NF- κ B (serine 536) in SB cells and FB cells were 68.84% and 45.64 % that of the control counterparts ($p = 0.013$ and $p = 0.005$; t -test), respectively (Figure 10A). However, phosphorylation status of c-JUN (a subunit of AP1), Akt and GSK3 β (downstream targets of the PI3K pathway) were unaffected by AEG-1 knockdown (Figure 11A). Also, the phosphorylation status of p65 at serine 468 and the level of phosphorylated I κ B are unchanged after AEG-1 knockdown in HNSCC cell lines (Figure 11B). These observations prompted us to examine the relationship between AEG-1 expression and the phosphorylation status of p65 at serine 536 in clinical specimens of HNSCC. A spatial correlation between AEG-1 and phosphorylated p65 was evident in the high AEG-1-expressing group, while the phosphorylated p65 signals in the low and nil AEG-1-expressing cases were primarily observed at the peripheral basal cells of the neoplastic nests (the location of AEG-1 proteins, Figure 10B). AEG-1, phosphorylated p65 and MMP1 were co-localized in the enrolled cohort of OSCC, and these associations were statistically significant (Figure 10C). Moreover, high levels of both phosphorylated p65 (serine 536) and MMP1 in neoplastic cells were positively associated with advanced tumor stages, as well as

with regional lymph node metastasis in OSCC (Tables 3 and 4). High MMP1 expression was also significantly associated with distant metastasis in our samples (Table 4).

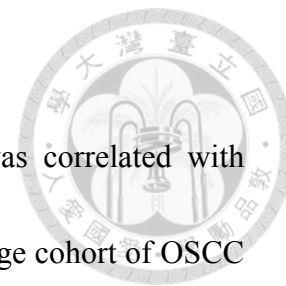


As AEG-1 was proposed as a single transmembrane protein expressed on the cell membrane and ER, we were interested in its subcellular distribution since our data suggested this protein to manipulate phosphorylation of p65. Transmission electron microscopy showed AEG-1 expression on the ER, Golgi apparatus, and cell membrane (Figures 13 and 14A). Also, flow cytometry assay using Lyric 4-7 antibody demonstrate the baseline expression of membranous AEG-1 is higher in FaDu cells than that in SAS cells, albeit a peak membranous AEG-1 expression is present in a small fraction (approximately 5%) of SAS cells (Figure 14B). Furthermore, transmission electron microscopy revealed the nuclear translocation of AEG-1 protein (Figures 13 and 14A), suggesting that AEG-1 may not be restricted to the membrane and cytosol, as previously reported. To further validate the hypothesis that AEG-1 regulates MMP1 through NF- κ B, we generated various luciferase reporter vectors driven by different fragments of the MMP1 promoter region (P1, -4372 to +52; P2, -2471 to +52; P3, -2269 to +52; and P4, -521 to +52) and transfected these reporters into the test cells (Figure 15B). A dramatic reduction of relative luciferase activity was observed in SB and FB cells transfected with P1 and P2, as compared to that in



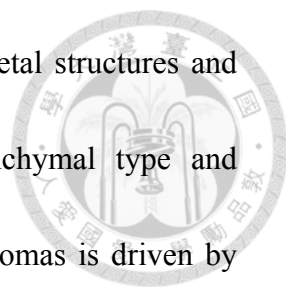
the respective controls; a smaller decrease was observed for knockdown cells transfected with P3, while luciferase activity was low in both knockdown and control cells transfected with P4 (Figure 15C). These results suggest that AEG-1 regulates elements between nucleotides -4372 to -2269 in the promoter of MMP1, where the binding sites of NF- κ B and CBP are located. CHIP revealed that AEG-1, p65 and CBP binding were reduced at the NF- κ B binding sequence of the MMP1 promoter in SB and FB cells as compared to that in the relevant controls, consistent with the data from our luciferase assay (Figure 15D). Taken together, these data suggest that AEG-1 increases phosphorylation of the p65 subunit of NF- κ B and regulates the expression of MMP1 in HNSCC cells.

Chapter IV: Discussion

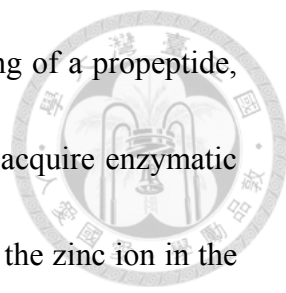


In this study, we found that high expression of AEG-1 was correlated with advanced tumor stages and regional lymph node metastasis in a large cohort of OSCC samples. The association between AEG-1 and distant metastasis was not statistically significant; evidence for an association may be confounded by the relatively low incidence (10%) of distant metastasis at initial presentation, a feature intrinsic to HNSCC [13]. In addition, our research has demonstrated that silencing of AEG-1 mitigates the malignant phenotypes of HNSCC cell lines *in vitro* and attenuates tumor growth and pulmonary metastasis *in vivo*. Our results provide the first strong evidence that AEG-1 is overexpressed in at least a subset of HNSCC and contributes to adverse clinical outcomes. Moreover, we found that AEG-1 upregulates the expression of MMP1, thereby uncovering a novel mechanism underlying the invasiveness of HNSCC.

Metastasis, defined as the detachment of daughter cells from the primary site of lesions and subsequent colonization of preferential target organs, is one of the hallmarks of malignancies [76, 77]. The metastasis cascade can be divided into steps of local invasion, intravasation, survival, extravasation and colonization. The tumor cells disseminate as individual cells, referred to as “individual cell migration”, or expand in solid cell strands, sheets, files and clusters, called “collective cell

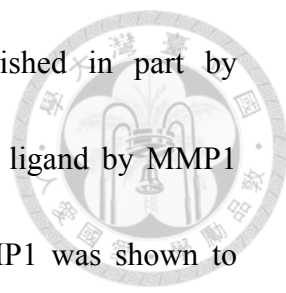


migration” [78]. Base on cell type, integrin engagement, cytoskeletal structures and protease production, single-cell migration can occur in mesenchymal type and amoeboid type. Mesenchymal type single cell migration in carcinomas is driven by epithelial-mesenchymal transition. Cells that undergo mesenchymal migration assume a spindle fibroblast-like morphology that is dependent on integrin-mediated adhesion dynamics and the presence of high traction force on both cell pole [79, 80]. Focal contacts form and turnover in the range of 10-120 min, resulting in relatively slow migration speeds of 0.1-2 $\mu\text{m}/\text{min}$ in 3D models [80, 81]. However, oral squamous cell carcinomas exhibit predominantly collective cell invasion [82]. Our data also revealed though knockdown of AEG-1 impeded migration and invasion of HNSCC cells, the EMT-related genes were unaffected in majority. There are three hallmarks that characterize collective cell migration. First, the cells remain physically and functionally connected such that the integrity of cell-cell junctions is preserved during movement [83, 84]. Second, multicellular polarity and organization of actin generate traction and protrusion force for migration and maintain cell-cell junctions. Finally, moving cell groups structurally modify the tissue along the migration path, either clearing the track or by causing secondary modification of extracellular matrix (ECM). Degradation and remodeling of ECM are essential for neoplastic permeation into adjacent stomal tissue, as well as for breaching the perivascular basement membrane

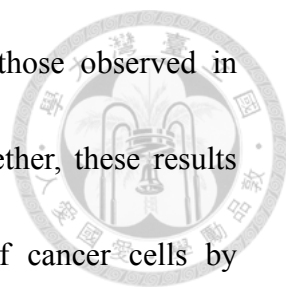


to initiate metastasis. MMPs are zinc-dependent enzymes, consisting of a propeptide, catalytic domain and a hemplexin-like C terminal domain. MMPs acquire enzymatic activity after peptidyl cleavage of the propeptide that interacts with the zinc ion in the catalytic domain [85]. The role of MMPs was traditionally believed to be primarily restricted to degradation of the ECM; however, mounting evidence suggests that MMPs are also involved in development, angiogenesis, inflammation and cancer progression, with the latter of which occurs through promoting migration and survival of cancer cells, orchestrating release of growth factors from extracellular reservoirs, and modulating recruitment of inflammatory cells to the tumor [86-88].

MMP1 is the stereotypical secreted collagenase of the MMP family, with its principle interstitial substrates consisting collagen I, II, III, VII, VIII, X, and gelatin. During collective cellular migration, which is the predominant pattern adopted by squamous cell carcinoma [89], MMP1 interacts with integrin $\alpha 2\beta 1$ at the leading edge [90], and degrades native matrix macromolecules into fragments that are subsequently processed by the gelatinases MMP2 and MMP9 [91]. Analyses of clinical specimens revealed that expression of MMP1 correlated with lymphatic invasion and lymph node metastasis [92, 93]. Furthermore, it is thought that MMP1 not only plays a pivotal role in vascular extravasation of metastatic neoplastic lesion, but it also contributes to the vascular remodeling at distant target sites, such as lung and bones

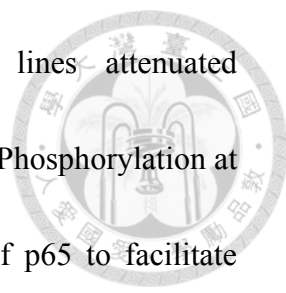


[94-96]. Promotion of osteotropic metastasis can be accomplished in part by activation of the RANKL pathway through cleavage of EGF-like ligand by MMP1 [97]. In addition to classical function of matrix remodeling, MMP1 was shown to manipulate biological behavior through direct interaction with receptors on neoplastic cells. Protease-activated receptors (PARs) are tethered-ligand, G protein-coupled receptors that are activated by proteolytic cleavage of their extracellular domains and participate in tumor invasion by inducing cancer cell migration [98]. PAR1, the prototypic member of the PAR family, has been known to respond to serine proteases including thrombin [99], plasmin [100], and activated protein C [101]. PAR1 expression is increased in a number of cancers including breast, colon, and lung. Nonetheless, MMP1 was identified as a nonserine protease agonist of PAR1 through cleaving the receptor between amino acid residues arginine 41 and serine 42 to generate PAR1-dependent Ca^{2+} signals and subsequent cell migration of breast cancer cells [86]. This cleavage can not be performed by MMP2, 3, 7, or 9. In summary, MMP1 contributes to tumor invasion and metastasis by remodeling the matrix, and triggering the signaling cascades and crosstalk between neoplastic cells and adjacent interstitium. In our study, we have shown that AEG-1-knockdown SAS and FaDu cells reduce both the invasive ability of cancer cells (Figure 4D) and the expressions of MMP1 (Figure 7). Furthermore, MMP inhibitor is able to inhibit the invasive



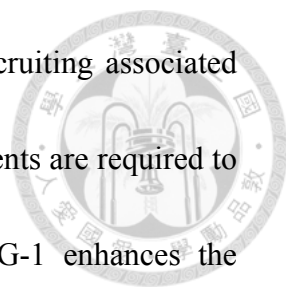
abilities of cancer cells (Figure 8) to the level comparable to those observed in AEG-1-knockdown SAS and FaDu cells (Figure 4D). Taken together, these results indicate that AEG-1 is able to increase the invasive ability of cancer cells by increasing MMP1 expression. It is also intriguing that MMP1 was demonstrated to converse pro-TNF- α into the soluble cytokinetic form through proteolytic cleavage [102]. TNF- α is a well-established positive upstream regulator of AEG-1 and it promotes cancer cell survival in an NF- κ B-dependent manner [103]. Combined with our data, it is suggested that AEG-1 function as a link in the vicious loop of TNF- α -NF- κ B axis.

To our knowledge, the present article is the first to report that AEG-1 regulates p65 phosphorylation at serine 536 and the subsequent MMP1 expression in HNSCC. MMP activity is modulated at various levels, including transcription, subcellular compartmentalization, proteolytic activation and inhibition. Data from our luciferase reporter assay indicate that AEG-1 regulates MMP1 transcription, primarily by acting on a region in the promoter upstream of nucleotide -2269. Previous studies reported the presence of NF- κ B and AP-1 binding sites at nucleotides -2886 and -3471 of the MMP1 promoter, respectively [75, 104]. Although AEG-1 has previously been reported to regulate MMP9 expression [64] through c-jun in human glioma cells [71], we found that AEG-1 does not affect phosphorylation of serines 63 and 73 of c-jun.



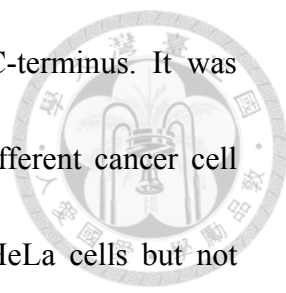
On the other hand, AEG-1 knockdown in HNSCC cell lines attenuated phosphorylation of the p65 subunit (RelA) of NF- κ B at serine 536. Phosphorylation at this amino acid residue is required for perinuclear localization of p65 to facilitate nuclear import [42, 105]. This observation was supported by the finding that AEG-1 expression correlates with phosphorylation of p65 at serine 536, both intertumorally and intratumorally, in OSCC clinical specimens ($p < 0.001$, Fisher's exact test). It was thought that the activation of NF- κ B requires degradation of I κ B. However, post-translational modifications of the subunits of NF- κ B have also been found to determine the functional activity to a great extent. Serine 536 of p65, which is located within the C-terminal transactivation domain, is a target of multiple protein kinases, including I κ B kinase α/β (IKK α/β), IKK ϵ , TANK binding kinase 1 (TBK1), and ribosomal S6 kinase 1 (RSK1). Phosphorylation at this amino acid residue has also been reported to suppress nuclear export of NF- κ B and to increase transactivation of a variety of downstream genes through positive interaction of p65 with co-activators (CBP and p300) [106-110]. Phosphorylation of serine 536 also activates the survival-promoting pathway when cells are challenged with chemotherapeutic cytotoxic agents such as doxorubicin and etoposide. [105, 111]

As mentioned previously, AEG-1 contains no known functional domains, making it unlikely that AEG-1 phosphorylates p65 directly. Based on our findings, it



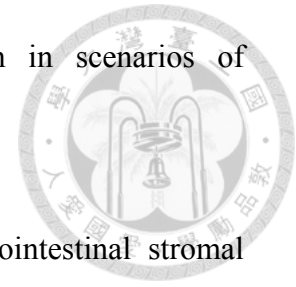
seems plausible that AEG-1 enhances p65 phosphorylation by recruiting associated protein kinases to the AEG-1-p65 complex. More detailed experiments are required to confirm this hypothesis. Our ChIP data also revealed that AEG-1 enhances the binding of p65 to the MMP1 promoter, thereby activating downstream genes by functioning as a linker between p65 and CBP to form the basal transcriptional machinery. Although p65 has been suggested to bind to AEG-1 through amino acid residues 101 to 205 of the latter [46], the interacting regions of CBP and AEG-1 remain unknown. Elucidation of the exact binding epitopes will require examination of the crystal structure of AEG-1 and its associated proteins.

Microarray analysis of the gene expression profile in SAS cell line revealed that MMP1 was not the sole gene under the influence of AEG-1. SNORD3B-1 (small nucleolar RNA, C/D box 3B-1), the gene that is up-regulated with high fold change after AEG-1 knockdown, is believed to function in RNA transport and ribosome biogenesis in eukaryocytes. However, no correlation between SNORD3B-1 and cancer biology has been documented in literatures. Initially isolated in 2001, Elastin microfibril interface located protein 2 (EMILIN2) is a relatively new member of the EMILIN family [112]. It is composed of the cysteine-rich EMI domain at the N-terminus, which is the hallmark of the family, α -helical domains with high probability for coiled-coil structure formation, and a proline-rich motif adjacent to a

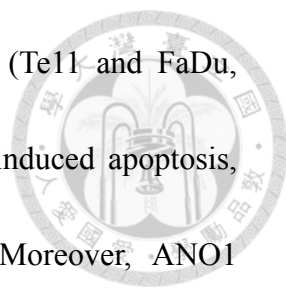


collagenous stalk preceding the globular gC1q domain at the C-terminus. It was shown that expression of EMILIN2 triggered the apoptosis of different cancer cell lines including HT1080 cells (a cell line of fibrosarcoma) and HeLa cells but not normal dermal fibroblasts [113]. Cell death depends on the activation of the extrinsic apoptotic pathway following EMILIN2 binding to the TRAIL receptors DR4 and, to a lesser extent, DR5. Binding is followed by receptor clustering and colocalization with lipid rafts occurred subsequently and lead to assembly of death-inducing signaling complex as well as caspase activation. The knockdown of EMILIN2 increased transformed cell survival, and overexpression impaired clonogenicity in soft agar and three-dimensional growth in natural matrices due to massive apoptosis. The domain responsible for triggering apoptosis of neoplastic cells was mapped to be between amino acid residues 286 to 436, a coiled-coil fragment toward the N-terminus of the molecule [114]. In addition to apoptosis-inducing capability on cancer cells, an increased tumor vessels density in the tumors treated with EMILIN2 was observed while tumor growth was significantly suppressed. Further studies showed that treatment with EMILIN2 failed to alter endothelial tubules formation in Matrigel, the protein significantly increased proliferation rate and migration of endothelial cells both in transwell system and in scratch tests. Combined the current findings with previous studies [74], it is evident that AEG-1 plays a role in remodeling

tumor-associated extracellular matrix and endothelial function in scenarios of angiogenesis and vascular damage.

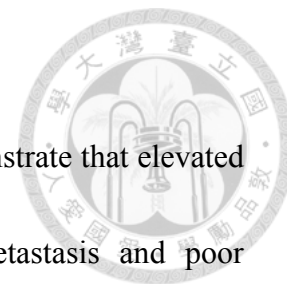


Anoctamin-1 (ANO1), also known as discovered on gastrointestinal stromal tumors protein 1 (DOG1), oral cancer overexpressed 2 (ORAOV2), tumor-amplified and overexpressed sequence 2 (TAOS2), and transmembrane proteins with unknown function 16 (TMEM16A), is upregulated in different cancer types, including gastrointestinal stromal tumor, squamous cell carcinoma of the upper aerodigestive tract and the esophagus (ESCC), and pancreatic cancer. ANO1 is a calcium-activated homodimerized chloride channel and the gene is located in chromosome 11q13 amplicon, where CCND1 (encoding cyclin D1) resides [115]. Amplification of a discrete, approximately 5-Mb region of 11q13 occurs in approximately one third of HNSCC, and it is even more prevalent in HPV-negative tumors [116, 117]. Although cyclin D1 has been considered to be the main driver of the 11q13 amplicon, it is not sufficient for malignant transformation of normal breast cells and lacks predictive value for the survival of HNSCC or breast cancer patients [118, 119]. A recent study demonstrated that ANO1 is amplified and highly expressed in cell lines and clinical specimen of breast cancer and HNSCC [120]. Amplification of ANO1 correlated with disease grade and poor prognosis in both disease entities. ANO1 is sufficient to promote cell viability in the absence of 11q13 amplification. Knockdown of ANO1 in



ANO1-amplified breast cancer cell lines and HNSCC cell lines (Te11 and FaDu, specifically) bearing 11q13 amplification inhibited proliferation, induced apoptosis, and reduced tumor growth in established cancer xenografts. Moreover, ANO1 chloride channel activity was indispensable for its prosurvival properties. Furthermore, ANO1 knockdown or pharmacological inhibition of its chloride-channel activity reduced EGF receptor (EGFR) and calmodulin-dependent protein kinase II (CAMKII) signaling, which subsequently attenuated AKT, v-src sarcoma viral oncogene homolog (SRC), and extracellular signal-regulated kinase (ERK) activation in breast cancer and HNSCC *in vitro* and *in vivo*. Validation of AEG-1 regulation upon ANO1 and elucidation of the underlying mechanism seems to be a promising topic for research and requires more detailed experiments.

Chapter V: Conclusion



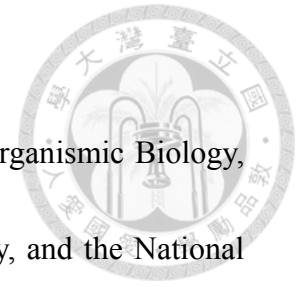
We used an extensive collection of HNSCC samples to demonstrate that elevated levels of AEG-1 protein are associated with lymph node metastasis and poor prognosis in HNSCC patients. AEG-1 primarily acts through the NF- κ B pathway, by enhancing phosphorylation on serine 536 of RelA, which in turn results in an increased expression of MMP1. These findings may support the development of AEG-1-targeting therapeutics, such as small molecules, interference RNA with suitable drug delivering system or DNA vaccine, [121] to bolster our arsenal of adjuvant chemotherapy, thereby improving the clinical outcome of HNSCC patients with high AEG-1 expression. In the meantime, elucidation of physiological function of AEG-1 through transgenic murine models and large-scale screening of the expression status of AEG-1 in normal human tissue are required to minimize the potential side effect.

Acknowledgements

We thank the Core Facility of the Institute of Cellular and Organismic Biology, the Microarray Core Facility of the Institute of Molecular Biology, and the National RNAi Core Facility, Academia Sinica for their generous and proficient technical support.

Funding

The current study was supported by the National Science Council, Taiwan, Grants NSC101-2325-B-001-010 and NSC101-2321-B-001-021 (to Han-Chung Wu), start-up funding for new faculty, National Taiwan university, Taipei, Taiwan, No.98R0616 and Professor Kwan's foundation, Taipei, Taiwan (to Yi-Ping Wang).



References

1. Jemal A, Bray F, Center MM, Ferlay J, Ward E, Forman D: **Global cancer statistics.** *CA Cancer J Clin* 2011, **61**:69-90.
2. Blot WJ, McLaughlin JK, Winn DM, Austin DF, Greenberg RS, Preston-Martin S, Bernstein L, Schoenberg JB, Stemhagen A, Fraumeni JF, Jr.: **Smoking and drinking in relation to oral and pharyngeal cancer.** *Cancer Res* 1988, **48**:3282-3287.
3. Tuyns AJ, Esteve J, Raymond L, Berrino F, Benhamou E, Blanchet F, Boffetta P, Crosignani P, del Moral A, Lehmann W, et al.: **Cancer of the larynx/hypopharynx, tobacco and alcohol: IARC international case-control study in Turin and Varese (Italy), Zaragoza and Navarra (Spain), Geneva (Switzerland) and Calvados (France).** *Int J Cancer* 1988, **41**:483-491.
4. D'Souza G, Kreimer AR, Viscidi R, Pawlita M, Fakhry C, Koch WM, Westra WH, Gillison ML: **Case-control study of human papillomavirus and oropharyngeal cancer.** *N Engl J Med* 2007, **356**:1944-1956.
5. Kreimer AR, Clifford GM, Boyle P, Franceschi S: **Human papillomavirus types in head and neck squamous cell carcinomas worldwide: a systematic review.** *Cancer Epidemiol Biomarkers Prev* 2005, **14**:467-475.
6. Hobbs CG, Sterne JA, Bailey M, Heyderman RS, Birchall MA, Thomas SJ: **Human papillomavirus and head and neck cancer: a systematic review and meta-analysis.** *Clin Otolaryngol* 2006, **31**:259-266.
7. Leemans CR, Tiwari R, Nauta JJ, van der Waal I, Snow GB: **Regional lymph node involvement and its significance in the development of distant metastases in head and neck carcinoma.** *Cancer* 1993, **71**:452-456.
8. Karamouzis MV, Grandis JR, Argiris A: **Therapies directed against epidermal growth factor receptor in aerodigestive carcinomas.** *JAMA* 2007, **298**:70-82.
9. Burtness B, Goldwasser MA, Flood W, Mattar B, Forastiere AA: **Phase III randomized trial of cisplatin plus placebo compared with cisplatin plus cetuximab in metastatic/recurrent head and neck cancer: an Eastern Cooperative Oncology Group study.** *J Clin Oncol* 2005, **23**:8646-8654.
10. Vermorken JB, Trigo J, Hitt R, Koralewski P, Diaz-Rubio E, Rolland F, Knecht R, Amellal N, Schueler A, Baselga J: **Open-label, uncontrolled, multicenter phase II study to evaluate the efficacy and toxicity of cetuximab as a single agent in patients with recurrent and/or metastatic squamous cell carcinoma of the head and neck who failed to respond to**

- platinum-based therapy.** *J Clin Oncol* 2007, **25**:2171-2177.
11. Argiris A, Brockstein BE, Haraf DJ, Stenson KM, Mittal BB, Kies MS, Rosen FR, Jovanovic B, Vokes EE: **Competing causes of death and second primary tumors in patients with locoregionally advanced head and neck cancer treated with chemoradiotherapy.** *Clin Cancer Res* 2004, **10**:1956-1962.
 12. Khuri FR, Lee JJ, Lippman SM, Kim ES, Cooper JS, Benner SE, Winn R, Pajak TF, Williams B, Shenouda G, et al: **Randomized phase III trial of low-dose isotretinoin for prevention of second primary tumors in stage I and II head and neck cancer patients.** *J Natl Cancer Inst* 2006, **98**:441-450.
 13. Argiris A, Karamouzis MV, Raben D, Ferris RL: **Head and neck cancer.** *Lancet* 2008, **371**:1695-1709.
 14. Su ZZ, Kang DC, Chen Y, Pekarskaya O, Chao W, Volsky DJ, Fisher PB: **Identification and cloning of human astrocyte genes displaying elevated expression after infection with HIV-1 or exposure to HIV-1 envelope glycoprotein by rapid subtraction hybridization, RaSH.** *Oncogene* 2002, **21**:3592-3602.
 15. Brown DM, Ruoslahti E: **Metadherin, a cell surface protein in breast tumors that mediates lung metastasis.** *Cancer Cell* 2004, **5**:365-374.
 16. Britt DE, Yang DF, Yang DQ, Flanagan D, Callanan H, Lim YP, Lin SH, Hixson DC: **Identification of a novel protein, LYRIC, localized to tight junctions of polarized epithelial cells.** *Exp Cell Res* 2004, **300**:134-148.
 17. Kang DC, Su ZZ, Sarkar D, Emdad L, Volsky DJ, Fisher PB: **Cloning and characterization of HIV-1-inducible astrocyte elevated gene-1, AEG-1.** *Gene* 2005, **353**:8-15.
 18. Sutherland HG, Lam YW, Briers S, Lamond AI, Bickmore WA: **3D3/lyric: a novel transmembrane protein of the endoplasmic reticulum and nuclear envelope, which is also present in the nucleolus.** *Exp Cell Res* 2004, **294**:94-105.
 19. Thirkettle HJ, Girling J, Warren AY, Mills IG, Sahadevan K, Leung H, Hamdy F, Whitaker HC, Neal DE: **LYRIC/AEG-1 is targeted to different subcellular compartments by ubiquitylation and intrinsic nuclear localization signals.** *Clin Cancer Res* 2009, **15**:3003-3013.
 20. Hornbeck PV, Kornhauser JM, Tkachev S, Zhang B, Skrzypek E, Murray B, Latham V, Sullivan M: **PhosphoSitePlus: a comprehensive resource for investigating the structure and function of experimentally determined post-translational modifications in man and mouse.** *Nucleic Acids Res* 2012, **40**:D261-270.

21. Xue Y, Ren J, Gao X, Jin C, Wen L, Yao X: **GPS 2.0, a tool to predict kinase-specific phosphorylation sites in hierarchy.** *Mol Cell Proteomics* 2008, **7**:1598-1608.
22. Su ZZ, Chen Y, Kang DC, Chao W, Simm M, Volsky DJ, Fisher PB: **Customized rapid subtraction hybridization (RaSH) gene microarrays identify overlapping expression changes in human fetal astrocytes resulting from human immunodeficiency virus-1 infection or tumor necrosis factor-alpha treatment.** *Gene* 2003, **306**:67-78.
23. Carnemolla A, Fossale E, Agostoni E, Michelazzi S, Calligaris R, De Maso L, Del Sal G, MacDonald ME, Persichetti F: **Rrs1 is involved in endoplasmic reticulum stress response in Huntington disease.** *J Biol Chem* 2009, **284**:18167-18173.
24. Lee SG, Su ZZ, Emdad L, Sarkar D, Fisher PB: **Astrocyte elevated gene-1 (AEG-1) is a target gene of oncogenic Ha-ras requiring phosphatidylinositol 3-kinase and c-Myc.** *Proc Natl Acad Sci U S A* 2006, **103**:17390-17395.
25. Noch E, Bookland M, Khalili K: **Astrocyte-elevated gene-1 (AEG-1) induction by hypoxia and glucose deprivation in glioblastoma.** *Cancer Biol Ther* 2011, **11**:32-39.
26. Khuda, II, Koide N, Noman AS, Dagvadorj J, Tumurkhuu G, Naiki Y, Komatsu T, Yoshida T, Yokochi T: **Astrocyte elevated gene-1 (AEG-1) is induced by lipopolysaccharide as toll-like receptor 4 (TLR4) ligand and regulates TLR4 signalling.** *Immunology* 2009, **128**:e700-706.
27. Zhang B, Liu XX, He JR, Zhou CX, Guo M, He M, Li MF, Chen GQ, Zhao Q: **Pathologically decreased miR-26a antagonizes apoptosis and facilitates carcinogenesis by targeting MTDH and EZH2 in breast cancer.** *Carcinogenesis* 2011, **32**:2-9.
28. Li J, Chen Y, Zhao J, Kong F, Zhang Y: **miR-203 reverses chemoresistance in p53-mutated colon cancer cells through downregulation of Akt2 expression.** *Cancer Lett* 2011, **304**:52-59.
29. Li J, Zhang Y, Zhao J, Kong F, Chen Y: **Overexpression of miR-22 reverses paclitaxel-induced chemoresistance through activation of PTEN signaling in p53-mutated colon cancer cells.** *Mol Cell Biochem* 2011, **357**:31-38.
30. Nohata N, Hanazawa T, Kikkawa N, Mutallip M, Sakurai D, Fujimura L, Kawakami K, Chiyomaru T, Yoshino H, Enokida H, et al: **Tumor suppressive microRNA-375 regulates oncogene AEG-1/MTDH in head and neck squamous cell carcinoma (HNSCC).** *J Hum Genet* 2011, **56**:595-601.
31. He XX, Chang Y, Meng FY, Wang MY, Xie QH, Tang F, Li PY, Song YH, Lin

- JS: **MicroRNA-375 targets AEG-1 in hepatocellular carcinoma and suppresses liver cancer cell growth in vitro and in vivo.** *Oncogene* 2012, **31**:3357-3369.
32. Hui AB, Bruce JP, Alajez NM, Shi W, Yue S, Perez-Ordóñez B, Xu W, O'Sullivan B, Waldron J, Cummings B, et al: **Significance of dysregulated metadherin and microRNA-375 in head and neck cancer.** *Clin Cancer Res* 2011, **17**:7539-7550.
33. Isozaki Y, Hoshino I, Nohata N, Kinoshita T, Akutsu Y, Hanari N, Mori M, Yoneyama Y, Akanuma N, Takeshita N, et al: **Identification of novel molecular targets regulated by tumor suppressive miR-375 induced by histone acetylation in esophageal squamous cell carcinoma.** *Int J Oncol* 2012, **41**:985-994.
34. Ward A, Balwierz A, Zhang JD, Kublbeck M, Pawitan Y, Hielscher T, Wiemann S, Sahin O: **Re-expression of microRNA-375 reverses both tamoxifen resistance and accompanying EMT-like properties in breast cancer.** *Oncogene* 2013, **32**:1173-1182.
35. Yang Y, Wu J, Guan H, Cai J, Fang L, Li J, Li M: **MiR-136 promotes apoptosis of glioma cells by targeting AEG-1 and Bcl-2.** *FEBS Lett* 2012, **586**:3608-3612.
36. Ghosh S, May MJ, Kopp EB: **NF-kappa B and Rel proteins: evolutionarily conserved mediators of immune responses.** *Annu Rev Immunol* 1998, **16**:225-260.
37. Wan F, Lenardo MJ: **The nuclear signaling of NF-kappaB: current knowledge, new insights, and future perspectives.** *Cell Res* 2010, **20**:24-33.
38. O'Shea JM, Perkins ND: **Regulation of the RelA (p65) transactivation domain.** *Biochem Soc Trans* 2008, **36**:603-608.
39. Hayden MS, Ghosh S: **Shared principles in NF-kappaB signaling.** *Cell* 2008, **132**:344-362.
40. Salminen A, Paimela T, Suuronen T, Kaarniranta K: **Innate immunity meets with cellular stress at the IKK complex: regulation of the IKK complex by HSP70 and HSP90.** *Immunol Lett* 2008, **117**:9-15.
41. Kanarek N, Ben-Neriah Y: **Regulation of NF-kappaB by ubiquitination and degradation of the IkappaBs.** *Immunol Rev* 2012, **246**:77-94.
42. Moreno R, Sobotzik JM, Schultz C, Schmitz ML: **Specification of the NF-kappaB transcriptional response by p65 phosphorylation and TNF-induced nuclear translocation of IKK epsilon.** *Nucleic Acids Res* 2010, **38**:6029-6044.
43. Huang B, Yang XD, Lamb A, Chen LF: **Posttranslational modifications of**

- NF-kappaB: another layer of regulation for NF-kappaB signaling pathway.** *Cell Signal* 2010, **22**:1282-1290.
44. Ling J, Kumar R: **Crosstalk between NFkB and glucocorticoid signaling: a potential target of breast cancer therapy.** *Cancer Lett* 2012, **322**:119-126.
45. Emdad L, Sarkar D, Su ZZ, Randolph A, Boukerche H, Valerie K, Fisher PB: **Activation of the nuclear factor kappaB pathway by astrocyte elevated gene-1: implications for tumor progression and metastasis.** *Cancer Res* 2006, **66**:1509-1516.
46. Sarkar D, Park ES, Emdad L, Lee SG, Su ZZ, Fisher PB: **Molecular basis of nuclear factor-kappaB activation by astrocyte elevated gene-1.** *Cancer Res* 2008, **68**:1478-1484.
47. Lee SG, Kim K, Kegelman TP, Dash R, Das SK, Choi JK, Emdad L, Howlett EL, Jeon HY, Su ZZ, et al: **Oncogene AEG-1 promotes glioma-induced neurodegeneration by increasing glutamate excitotoxicity.** *Cancer Res* 2011, **71**:6514-6523.
48. Kikuno N, Shiina H, Urakami S, Kawamoto K, Hirata H, Tanaka Y, Place RF, Pookot D, Majid S, Igawa M, Dahiya R: **Knockdown of astrocyte-elevated gene-1 inhibits prostate cancer progression through upregulation of FOXO3a activity.** *Oncogene* 2007, **26**:7647-7655.
49. Emdad L, Lee SG, Su ZZ, Jeon HY, Boukerche H, Sarkar D, Fisher PB: **Astrocyte elevated gene-1 (AEG-1) functions as an oncogene and regulates angiogenesis.** *Proc Natl Acad Sci U S A* 2009, **106**:21300-21305.
50. Hennessy BT, Smith DL, Ram PT, Lu Y, Mills GB: **Exploiting the PI3K/AKT pathway for cancer drug discovery.** *Nat Rev Drug Discov* 2005, **4**:988-1004.
51. Engelman JA, Luo J, Cantley LC: **The evolution of phosphatidylinositol 3-kinases as regulators of growth and metabolism.** *Nat Rev Genet* 2006, **7**:606-619.
52. Vivanco I, Sawyers CL: **The phosphatidylinositol 3-Kinase AKT pathway in human cancer.** *Nat Rev Cancer* 2002, **2**:489-501.
53. Datta SR, Brunet A, Greenberg ME: **Cellular survival: a play in three Akts.** *Genes Dev* 1999, **13**:2905-2927.
54. Brunet A, Bonni A, Zigmond MJ, Lin MZ, Juo P, Hu LS, Anderson MJ, Arden KC, Blenis J, Greenberg ME: **Akt promotes cell survival by phosphorylating and inhibiting a Forkhead transcription factor.** *Cell* 1999, **96**:857-868.
55. Zhou BP, Liao Y, Xia W, Spohn B, Lee MH, Hung MC: **Cytoplasmic localization of p21Cip1/WAF1 by Akt-induced phosphorylation in**

- HER-2/neu-overexpressing cells.** *Nat Cell Biol* 2001, **3**:245-252.
56. Sherr CJ, Weber JD: **The ARF/p53 pathway.** *Curr Opin Genet Dev* 2000, **10**:94-99.
57. Lee SG, Su ZZ, Emdad L, Sarkar D, Franke TF, Fisher PB: **Astrocyte elevated gene-1 activates cell survival pathways through PI3K-Akt signaling.** *Oncogene* 2008, **27**:1114-1121.
58. Li J, Yang L, Song L, Xiong H, Wang L, Yan X, Yuan J, Wu J, Li M: **Astrocyte elevated gene-1 is a proliferation promoter in breast cancer via suppressing transcriptional factor FOXO1.** *Oncogene* 2009, **28**:3188-3196.
59. Yoo BK, Chen D, Su ZZ, Gredler R, Yoo J, Shah K, Fisher PB, Sarkar D: **Molecular mechanism of chemoresistance by astrocyte elevated gene-1.** *Cancer Res* 2010, **70**:3249-3258.
60. Yang J, Valineva T, Hong J, Bu T, Yao Z, Jensen ON, Frilander MJ, Silvennoinen O: **Transcriptional co-activator protein p100 interacts with snRNP proteins and facilitates the assembly of the spliceosome.** *Nucleic Acids Res* 2007, **35**:4485-4494.
61. Caudy AA, Ketting RF, Hammond SM, Denli AM, Bathoorn AM, Tops BB, Silva JM, Myers MM, Hannon GJ, Plasterk RH: **A micrococcal nuclease homologue in RNAi effector complexes.** *Nature* 2003, **425**:411-414.
62. Yoo BK, Santhekadur PK, Gredler R, Chen D, Emdad L, Bhutia S, Pannell L, Fisher PB, Sarkar D: **Increased RNA-induced silencing complex (RISC) activity contributes to hepatocellular carcinoma.** *Hepatology* 2011, **53**:1538-1548.
63. Blanco MA, Aleckovic M, Hua Y, Li T, Wei Y, Xu Z, Cristea IM, Kang Y: **Identification of staphylococcal nuclease domain-containing 1 (SND1) as a Metadherin-interacting protein with metastasis-promoting functions.** *J Biol Chem* 2011, **286**:19982-19992.
64. Emdad L, Sarkar D, Lee SG, Su ZZ, Yoo BK, Dash R, Yacoub A, Fuller CE, Shah K, Dent P, et al: **Astrocyte elevated gene-1: a novel target for human glioma therapy.** *Mol Cancer Ther* 2010, **9**:79-88.
65. Lee SG, Jeon HY, Su ZZ, Richards JE, Vozhilla N, Sarkar D, Van Maerken T, Fisher PB: **Astrocyte elevated gene-1 contributes to the pathogenesis of neuroblastoma.** *Oncogene* 2009, **28**:2476-2484.
66. Wang F, Ke ZF, Sun SJ, Chen WF, Yang SC, Li SH, Mao XP, Wang LT: **Oncogenic roles of astrocyte elevated gene-1 (AEG-1) in osteosarcoma progression and prognosis.** *Cancer Biol Ther* 2011, **12**:539-548.
67. Yoo BK, Emdad L, Su ZZ, Villanueva A, Chiang DY, Mukhopadhyay ND, Mills AS, Waxman S, Fisher RA, Llovet JM, et al: **Astrocyte elevated gene-1**

- regulates hepatocellular carcinoma development and progression.** *J Clin Invest* 2009, **119**:465-477.
68. Li J, Zhang N, Song LB, Liao WT, Jiang LL, Gong LY, Wu J, Yuan J, Zhang HZ, Zeng MS, Li M: **Astrocyte elevated gene-1 is a novel prognostic marker for breast cancer progression and overall patient survival.** *Clin Cancer Res* 2008, **14**:3319-3326.
69. Hu G, Chong RA, Yang Q, Wei Y, Blanco MA, Li F, Reiss M, Au JL, Haffty BG, Kang Y: **MTDH activation by 8q22 genomic gain promotes chemoresistance and metastasis of poor-prognosis breast cancer.** *Cancer Cell* 2009, **15**:9-20.
70. Song L, Li W, Zhang H, Liao W, Dai T, Yu C, Ding X, Zhang L, Li J: **Over-expression of AEG-1 significantly associates with tumour aggressiveness and poor prognosis in human non-small cell lung cancer.** *J Pathol* 2009, **219**:317-326.
71. Liu L, Wu J, Ying Z, Chen B, Han A, Liang Y, Song L, Yuan J, Li J, Li M: **Astrocyte elevated gene-1 upregulates matrix metalloproteinase-9 and induces human glioma invasion.** *Cancer Res* 2010, **70**:3750-3759.
72. Sun S, Ke Z, Wang F, Li S, Chen W, Han A, Wang Z, Shi H, Wang LT, Chen X: **Overexpression of astrocyte-elevated gene-1 is closely correlated with poor prognosis in human non-small cell lung cancer and mediates its metastasis through up-regulation of matrix metalloproteinase-9 expression.** *Hum Pathol* 2012, **43**:1051-1060.
73. Li X, Kong X, Huo Q, Guo H, Yan S, Yuan C, Moran MS, Shao C, Yang Q: **Metadherin enhances the invasiveness of breast cancer cells by inducing epithelial to mesenchymal transition.** *Cancer Sci* 2011, **102**:1151-1157.
74. Liu IJ, Chiu CY, Chen YC, Wu HC: **Molecular mimicry of human endothelial cell antigen by autoantibodies to nonstructural protein 1 of dengue virus.** *J Biol Chem* 2011, **286**:9726-9736.
75. Rutter JL, Benbow U, Coon CI, Brinckerhoff CE: **Cell-type specific regulation of human interstitial collagenase-1 gene expression by interleukin-1 beta (IL-1 beta) in human fibroblasts and BC-8701 breast cancer cells.** *J Cell Biochem* 1997, **66**:322-336.
76. Gupta GP, Massague J: **Cancer metastasis: building a framework.** *Cell* 2006, **127**:679-695.
77. Steeg PS: **Tumor metastasis: mechanistic insights and clinical challenges.** *Nat Med* 2006, **12**:895-904.
78. Friedl P, Wolf K: **Tumour-cell invasion and migration: diversity and escape mechanisms.** *Nat Rev Cancer* 2003, **3**:362-374.

79. Cukierman E, Pankov R, Stevens DR, Yamada KM: **Taking cell-matrix adhesions to the third dimension.** *Science* 2001, **294**:1708-1712.
80. Ballestrem C, Hinz B, Imhof BA, Wehrle-Haller B: **Marching at the front and dragging behind: differential α V β 3-integrin turnover regulates focal adhesion behavior.** *J Cell Biol* 2001, **155**:1319-1332.
81. Zamir E, Katz M, Posen Y, Erez N, Yamada KM, Katz BZ, Lin S, Lin DC, Bershadsky A, Kam Z, Geiger B: **Dynamics and segregation of cell-matrix adhesions in cultured fibroblasts.** *Nat Cell Biol* 2000, **2**:191-196.
82. Friedl P, Gilmour D: **Collective cell migration in morphogenesis, regeneration and cancer.** *Nat Rev Mol Cell Biol* 2009, **10**:445-457.
83. Montell DJ: **Morphogenetic cell movements: diversity from modular mechanical properties.** *Science* 2008, **322**:1502-1505.
84. Carmona-Fontaine C, Matthews HK, Kuriyama S, Moreno M, Dunn GA, Parsons M, Stern CD, Mayor R: **Contact inhibition of locomotion in vivo controls neural crest directional migration.** *Nature* 2008, **456**:957-961.
85. Gross J, Lapiere CM: **Collagenolytic activity in amphibian tissues: a tissue culture assay.** *Proc Natl Acad Sci U S A* 1962, **48**:1014-1022.
86. Boire A, Covic L, Agarwal A, Jacques S, Sherifi S, Kuliopulos A: **PAR1 is a matrix metalloproteinase-1 receptor that promotes invasion and tumorigenesis of breast cancer cells.** *Cell* 2005, **120**:303-313.
87. Yu Q, Stamenkovic I: **Cell surface-localized matrix metalloproteinase-9 proteolytically activates TGF-beta and promotes tumor invasion and angiogenesis.** *Genes Dev* 2000, **14**:163-176.
88. McQuibban GA, Gong JH, Wong JP, Wallace JL, Clark-Lewis I, Overall CM: **Matrix metalloproteinase processing of monocyte chemoattractant proteins generates CC chemokine receptor antagonists with anti-inflammatory properties in vivo.** *Blood* 2002, **100**:1160-1167.
89. Friedl P, Noble PB, Walton PA, Laird DW, Chauvin PJ, Tabah RJ, Black M, Zanker KS: **Migration of coordinated cell clusters in mesenchymal and epithelial cancer explants in vitro.** *Cancer Res* 1995, **55**:4557-4560.
90. Dumin JA, Dickeson SK, Stricker TP, Bhattacharyya-Pakrasi M, Roby JD, Santoro SA, Parks WC: **Pro-collagenase-1 (matrix metalloproteinase-1) binds the α (2) β (1) integrin upon release from keratinocytes migrating on type I collagen.** *J Biol Chem* 2001, **276**:29368-29374.
91. Deryugina EI, Bourdon MA, Reisfeld RA, Strongin A: **Remodeling of collagen matrix by human tumor cells requires activation and cell surface association of matrix metalloproteinase-2.** *Cancer Res* 1998, **58**:3743-3750.
92. Langenskiold M, Holmdahl L, Falk P, Ivarsson ML: **Increased plasma**

- MMP-2 protein expression in lymph node-positive patients with colorectal cancer.** *Int J Colorectal Dis* 2005, **20**:245-252.
93. Baker EA, Bergin FG, Leaper DJ: **Matrix metalloproteinases, their tissue inhibitors and colorectal cancer staging.** *Br J Surg* 2000, **87**:1215-1221.
94. Minn AJ, Gupta GP, Siegel PM, Bos PD, Shu W, Giri DD, Viale A, Olshen AB, Gerald WL, Massague J: **Genes that mediate breast cancer metastasis to lung.** *Nature* 2005, **436**:518-524.
95. Gupta GP, Nguyen DX, Chiang AC, Bos PD, Kim JY, Nadal C, Gomis RR, Manova-Todorova K, Massague J: **Mediators of vascular remodelling co-opted for sequential steps in lung metastasis.** *Nature* 2007, **446**:765-770.
96. Kang Y, Siegel PM, Shu W, Drobnjak M, Kakonen SM, Cordon-Cardo C, Guise TA, Massague J: **A multigenic program mediating breast cancer metastasis to bone.** *Cancer Cell* 2003, **3**:537-549.
97. Lu X, Wang Q, Hu G, Van Poznak C, Fleisher M, Reiss M, Massague J, Kang Y: **ADAMTS1 and MMP1 proteolytically engage EGF-like ligands in an osteolytic signaling cascade for bone metastasis.** *Genes Dev* 2009, **23**:1882-1894.
98. Coughlin SR: **Thrombin signalling and protease-activated receptors.** *Nature* 2000, **407**:258-264.
99. Vu TK, Hung DT, Wheaton VI, Coughlin SR: **Molecular cloning of a functional thrombin receptor reveals a novel proteolytic mechanism of receptor activation.** *Cell* 1991, **64**:1057-1068.
100. Kuliopulos A, Covic L, Seeley SK, Sheridan PJ, Helin J, Costello CE: **Plasmin desensitization of the PAR1 thrombin receptor: kinetics, sites of truncation, and implications for thrombolytic therapy.** *Biochemistry* 1999, **38**:4572-4585.
101. Riewald M, Petrovan RJ, Donner A, Mueller BM, Ruf W: **Activation of endothelial cell protease activated receptor 1 by the protein C pathway.** *Science* 2002, **296**:1880-1882.
102. Manicone AM, McGuire JK: **Matrix metalloproteinases as modulators of inflammation.** *Semin Cell Dev Biol* 2008, **19**:34-41.
103. Luo JL, Maeda S, Hsu LC, Yagita H, Karin M: **Inhibition of NF-kappaB in cancer cells converts inflammation- induced tumor growth mediated by TNFalpha to TRAIL-mediated tumor regression.** *Cancer Cell* 2004, **6**:297-305.
104. Maldonado A, Game BA, Song L, Huang Y: **Up-regulation of matrix metalloproteinase-1 expression in U937 cells by low-density lipoprotein-containing immune complexes requires the activator protein-1**

- and the Ets motifs in the distal and the proximal promoter regions. *Immunology* 2003, **109**:572-579.
105. Bohuslav J, Chen LF, Kwon H, Mu Y, Greene WC: **p53 induces NF-kappaB activation by an IkappaB kinase-independent mechanism involving phosphorylation of p65 by ribosomal S6 kinase 1.** *J Biol Chem* 2004, **279**:26115-26125.
106. Sakurai H, Chiba H, Miyoshi H, Sugita T, Toriumi W: **IkappaB kinases phosphorylate NF-kappaB p65 subunit on serine 536 in the transactivation domain.** *J Biol Chem* 1999, **274**:30353-30356.
107. O'Mahony AM, Montano M, Van Beneden K, Chen LF, Greene WC: **Human T-cell lymphotropic virus type 1 tax induction of biologically Active NF-kappaB requires IkappaB kinase-1-mediated phosphorylation of RelA/p65.** *J Biol Chem* 2004, **279**:18137-18145.
108. Jiang X, Takahashi N, Matsui N, Tetsuka T, Okamoto T: **The NF-kappa B activation in lymphotoxin beta receptor signaling depends on the phosphorylation of p65 at serine 536.** *J Biol Chem* 2003, **278**:919-926.
109. Buss H, Dorrie A, Schmitz ML, Hoffmann E, Resch K, Kracht M: **Constitutive and interleukin-1-inducible phosphorylation of p65 NF-kB at serine 536 is mediated by multiple protein kinases including IkB kinase IKK α , IKK β , IKK ϵ , TRAF family member-associated (TANK)-binding kinase 1 (TBK1), and an unknown kinase and couples p65 to TATA-binding protein-associated factor II31-mediated interleukin-8 transcription.** *J Biol Chem* 2004, **279**:55633-55643.
110. Fujita F, Taniguchi Y, Kato T, Narita Y, Furuya A, Ogawa T, Sakurai H, Joh T, Itoh M, Delhase M, et al: **Identification of NAP1, a regulatory subunit of IkappaB kinase-related kinases that potentiates NF-kappaB signaling.** *Mol Cell Biol* 2003, **23**:7780-7793.
111. Ho WC, Dickson KM, Barker PA: **Nuclear factor-kappaB induced by doxorubicin is deficient in phosphorylation and acetylation and represses nuclear factor-kappaB-dependent transcription in cancer cells.** *Cancer Res* 2005, **65**:4273-4281.
112. Doliana R, Bot S, Mungiguerra G, Canton A, Cilli SP, Colombatti A: **Isolation and characterization of EMILIN-2, a new component of the growing EMILINs family and a member of the EMI domain-containing superfamily.** *J Biol Chem* 2001, **276**:12003-12011.
113. Mongiat M, Ligresti G, Marastoni S, Lorenzon E, Doliana R, Colombatti A: **Regulation of the extrinsic apoptotic pathway by the extracellular matrix glycoprotein EMILIN2.** *Mol Cell Biol* 2007, **27**:7176-7187.

114. Mongiat M, Marastoni S, Ligresti G, Lorenzon E, Schiappacassi M, Perris R, Frustaci S, Colombatti A: **The extracellular matrix glycoprotein elastin microfibril interface located protein 2: a dual role in the tumor microenvironment.** *Neoplasia* 2010, **12**:294-304.
115. Huang F, Wong X, Jan LY: **International Union of Basic and Clinical Pharmacology. LXXXV: calcium-activated chloride channels.** *Pharmacol Rev* 2012, **64**:1-15.
116. Smeets SJ, Braakhuis BJ, Abbas S, Snijders PJ, Ylstra B, van de Wiel MA, Meijer GA, Leemans CR, Brakenhoff RH: **Genome-wide DNA copy number alterations in head and neck squamous cell carcinomas with or without oncogene-expressing human papillomavirus.** *Oncogene* 2006, **25**:2558-2564.
117. Sheu JJ, Hua CH, Wan L, Lin YJ, Lai MT, Tseng HC, Jinawath N, Tsai MH, Chang NW, Lin CF, et al: **Functional genomic analysis identified epidermal growth factor receptor activation as the most common genetic event in oral squamous cell carcinoma.** *Cancer Res* 2009, **69**:2568-2576.
118. Rodrigo JP, Garcia-Carracedo D, Garcia LA, Menendez S, Allonca E, Gonzalez MV, Fresno MF, Suarez C, Garcia-Pedrero JM: **Distinctive clinicopathological associations of amplification of the cortactin gene at 11q13 in head and neck squamous cell carcinomas.** *J Pathol* 2009, **217**:516-523.
119. Debnath J, Mills KR, Collins NL, Reginato MJ, Muthuswamy SK, Brugge JS: **The role of apoptosis in creating and maintaining luminal space within normal and oncogene-expressing mammary acini.** *Cell* 2002, **111**:29-40.
120. Britschgi A, Bill A, Brinkhaus H, Rothwell C, Clay I, Duss S, Rebhan M, Raman P, Guy CT, Wetzel K, et al: **Calcium-activated chloride channel ANO1 promotes breast cancer progression by activating EGFR and CAMK signaling.** *Proc Natl Acad Sci U S A* 2013, **110**:E1026-1034.
121. Qian BJ, Yan F, Li N, Liu QL, Lin YH, Liu CM, Luo YP, Guo F, Li HZ: **MTDH/AEG-1-based DNA vaccine suppresses lung metastasis and enhances chemosensitivity to doxorubicin in breast cancer.** *Cancer Immunol Immunother* 2011, **60**:883-893.

Figures

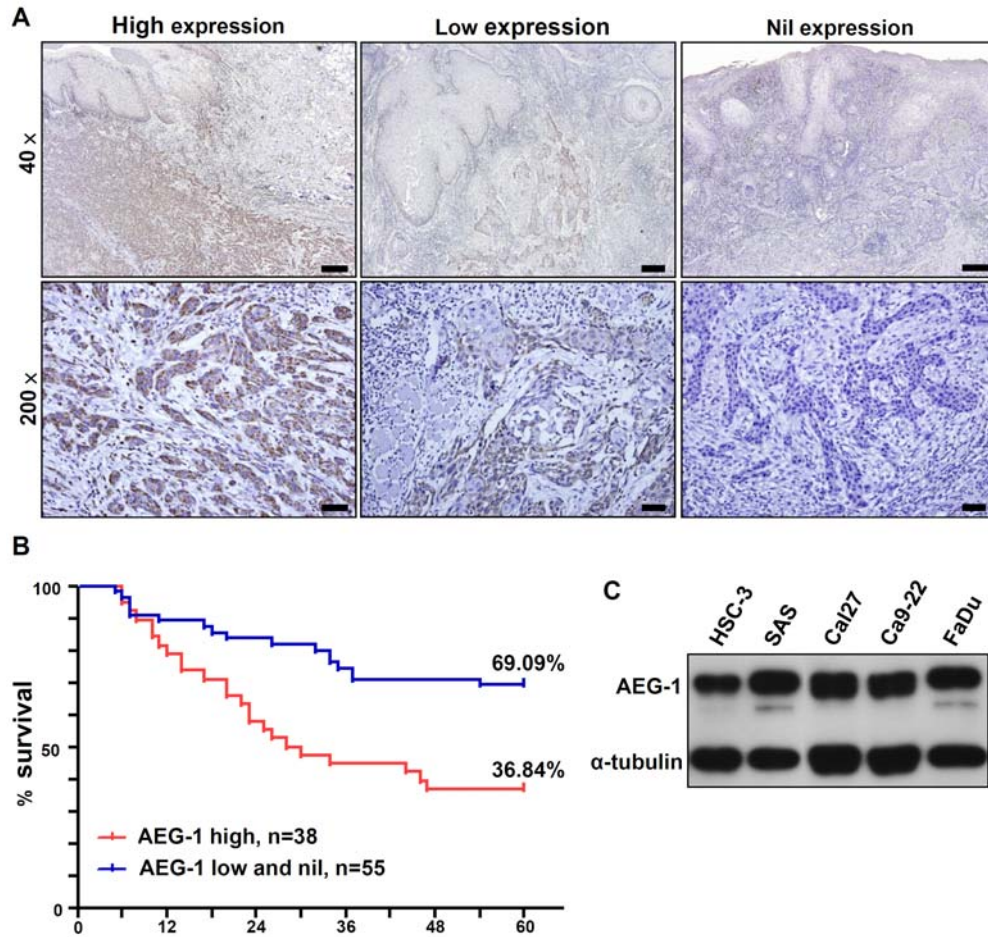


Figure 1. AEG-1 expression in clinical specimens of OSCC and cell lines of HNSCC. (A) immunohistochemical staining of formalin-fixed, paraffin embedded OSCC specimens. Scale bar: 40 \times , 300 μ m; 200 \times , 45 μ m. (B) Kaplan-Meier 5-year survival analysis of 93 cases of OSCC segregated by expression status of AEG-1 protein. (C) AEG-1 protein expression in HNSCC cell lines.

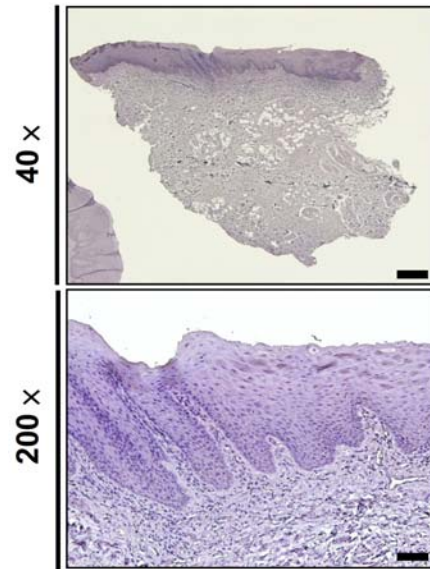
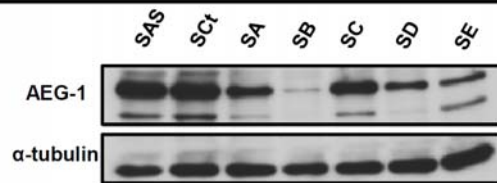


Figure 2. Immunohistochemical staining of LYRIC in 30 cases of normal uninflamed oral mucosa. No positive signal of LYRIC is discerned in the surface mucosa keratinocytes. Scale bar: 40 ×, 300 μm; 200 ×, 45 μm.



A

Clone ID	Oligosequence
AEG-1 shRNA-A	CCGGGCAACTTACAACCGCATCATTCTCGAGAATGATGCGGTTGTAAGTTGCTTTTTTG
AEG-1 shRNA-B	CCGGCGAGGAATAAAGGATTCTGATCTCGAGATCAGAATCCTTTATTCCTCGTTTTTTG
AEG-1 shRNA-C	CCGGGCCTTATTAATGGACAGCTTTCTCGAGAAAGCTGTCCATTAATAAGGCTTTTTTTG
AEG-1 shRNA-D	CCGGCCAAGTCAAATACCAAGCAAACCTCGAGTTTGCTTGGTATTTGACTTGGTTTTTTG
AEG-1 shRNA-E	CCGGCGATGATGAATGGTCTGGTTCTCGAGAACCCAGACCATTTCATCATCGTTTTTTG



B

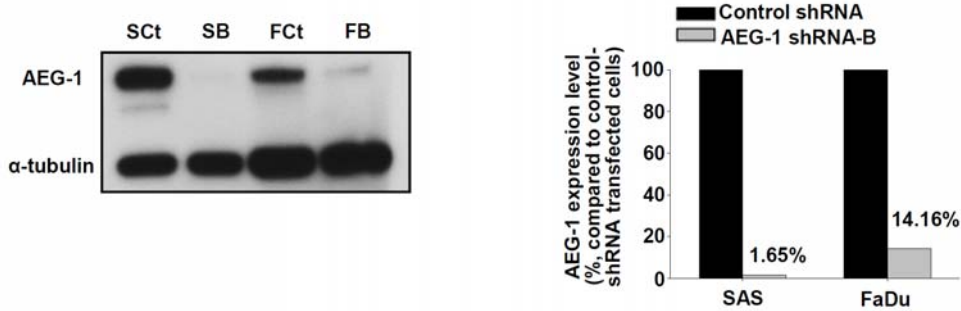


Figure 3. Establishment of stable clones of AEG-1-knockdown HNSCC cell lines. (A) upper, sequences of shRNA targeting to AEG-1mRNA; lower, AEG-1 protein expression in SAS cells after transfection of shRNA. (B) Western blotting of total cell lysates from both cell lines transfected with lentiviral AEG-1-specific shRNA showed efficient AEG-1 suppression in protein level in SAS and FaDu cells (1.65% and 14.16% respectively, normalized with the expression levels of α -tubulin).

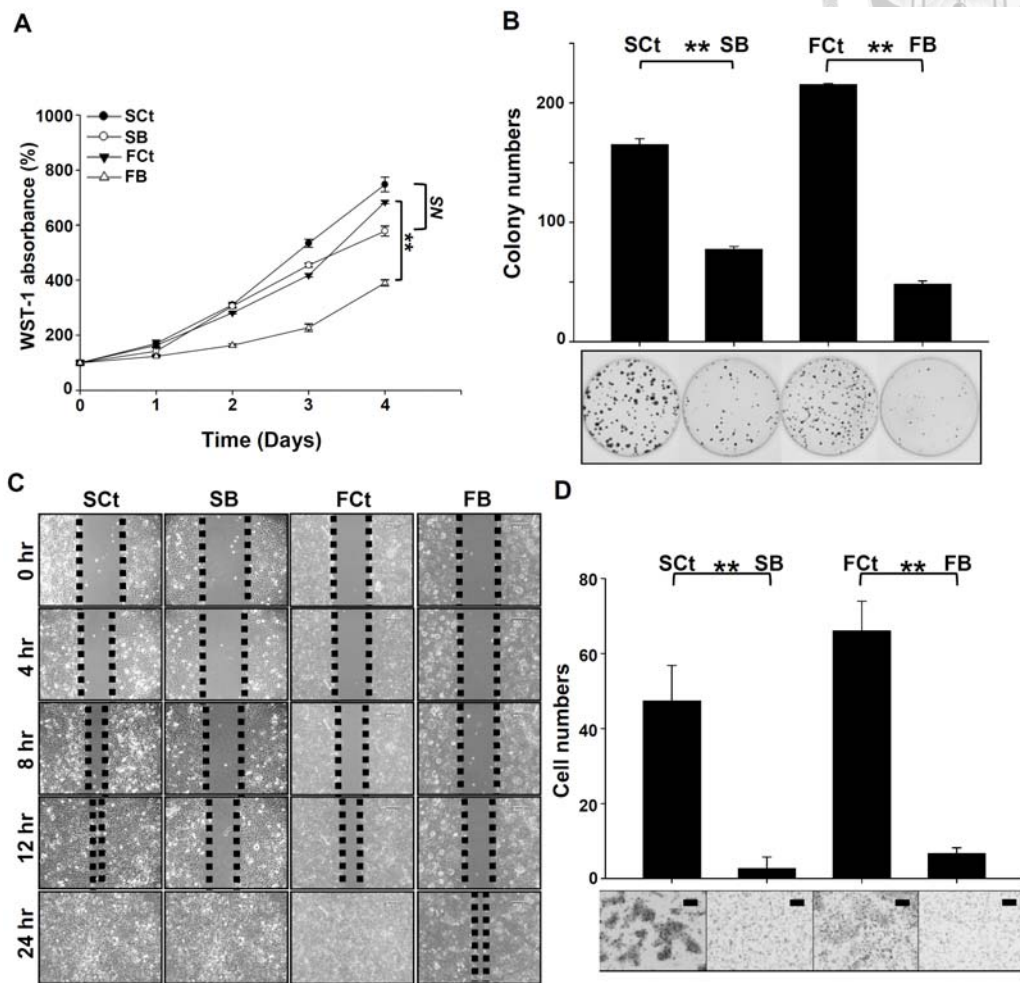


Figure 4. Impact of AEG-1 knockdown on the function of HNSCC cell lines. (A) WST-1 cell proliferation assay. (B) colony formation assay. (C) wound-healing migration assay. Initial gap: 500 μm. (D) transwell Matrigel invasion assay. All values are the average of three independent experiments. SB, AEG-1 knockdown SAS cells. FB, AEG-1 knockdown FaDu cells. SCt, SAS cells transfected with scrambled control shRNA. FCt, FaDu cells transfected with scrambled control shRNA. All data were expressed as mean ± SEM; n = 3. NS, not significant ($p > 0.05$); **, $p < 0.01$. Scale Bar: 130 μm.

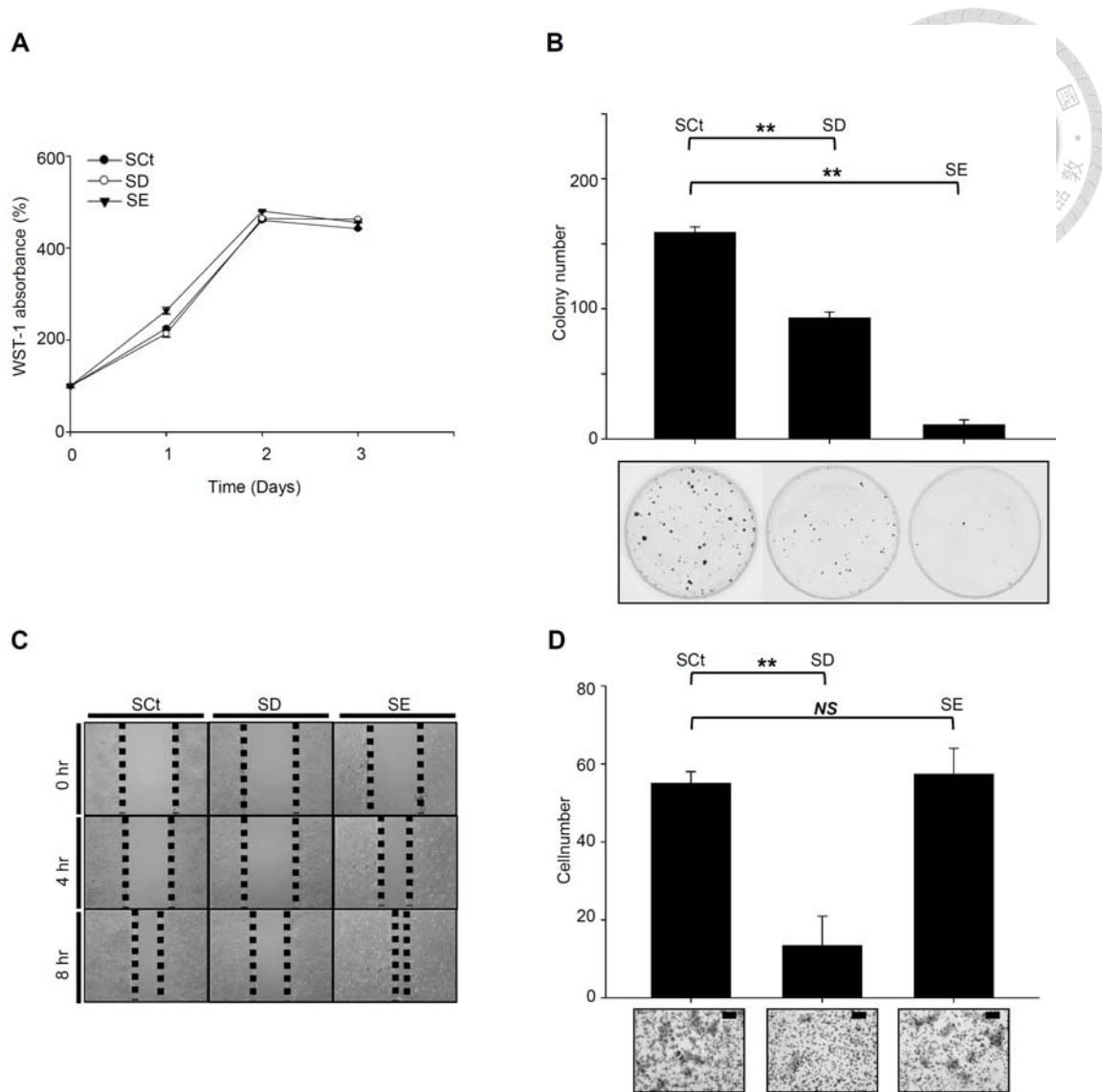


Figure 5. Impact of AEG-1 knockdown on the function of SAS cell line. (A) WST-1 cell proliferation assay. (B) colony formation assay. (C) wound healing migration assay. Initial gap: 500 μm. (D) transwell Matrigel invasion assay. All values are the average of three independent experiments. SCt, SAS cells transfected with scrambled control shRNA; SB, SD, and SE, AEG-1 knockdown stable clone SAS cells. NS, not significant ($p > 0.05$); **, $p < 0.01$. Scale Bar: 130 μm.

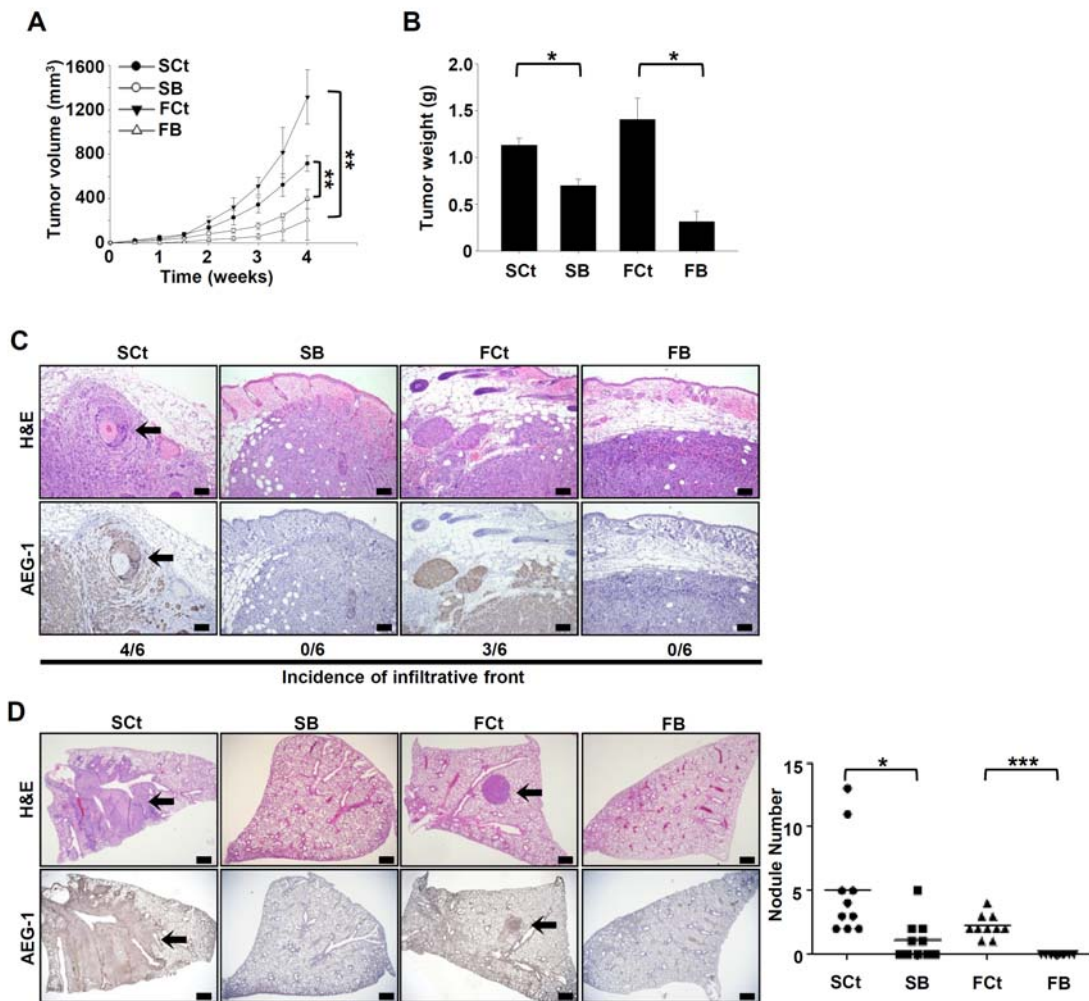


Figure 6. AEG-1 knockdown compromises tumorigenicity ($n = 6$) and pulmonary metastasis ($n = 10$) of SAS and FaDu cells. (A) time-course plot of tumor volumes. (B) tumor weights at the end-point. *, $p < 0.05$; **, $p < 0.01$. (C) microscopy images of xenograft tumors at the end-point. Note the infiltrated invasion fronts in the SCt and FCt groups and the expansile tumor borders in the SB and FB groups. Arrow, focus of perineural invasion. Upper row, H&E stain; lower row, immunohistochemical stain with Lyric 4-7. Scale bar, 100 μm . (D) In vivo lung metastasis assay. Arrow, metastatic focus. Upper row, H&E stain; lower row, immunohistochemical stain with anti-AEG-1 antibody. Scale bar, 500 μm .

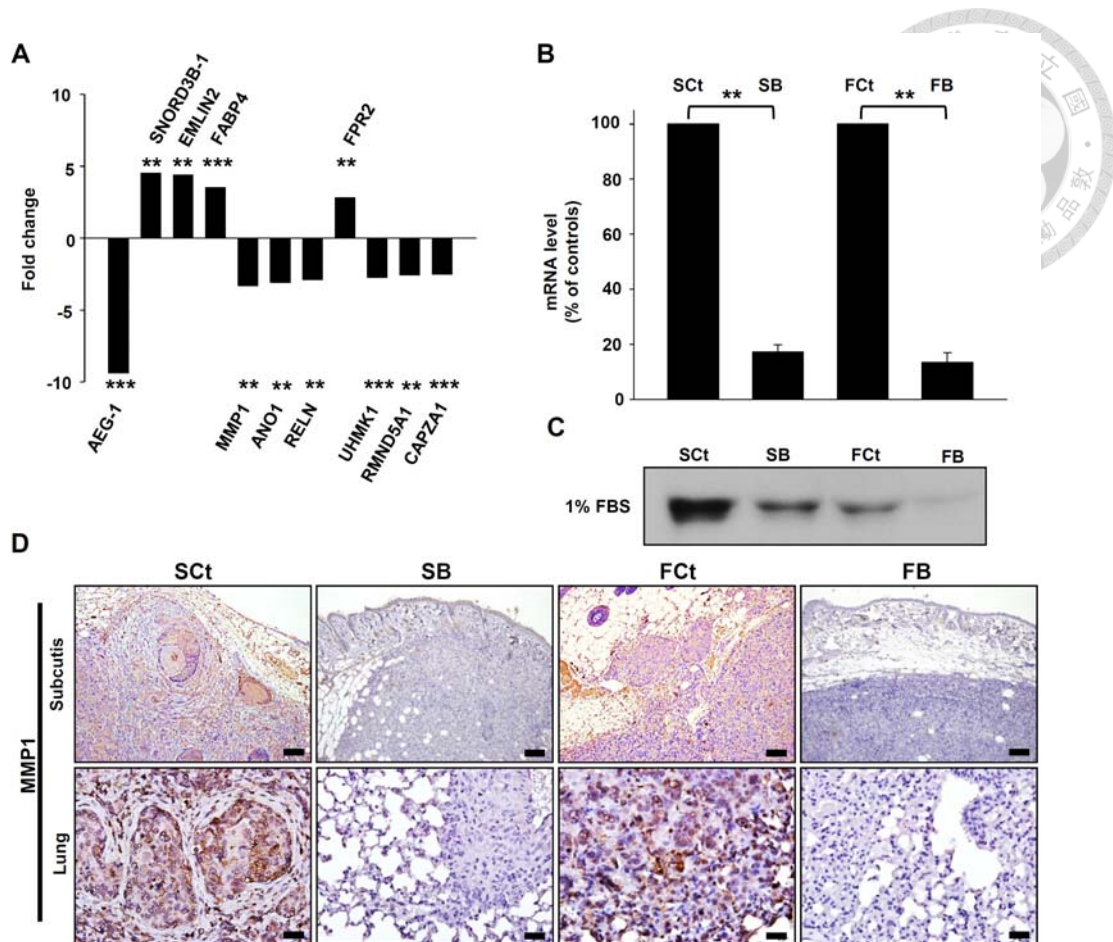


Figure 7. AEG-1 knockdown down-regulated MMP1 expression in HNSCC cells *in vitro* and *in vivo*. (A) microarray analysis of gene expression after AEG-1 knockdown in SAS cells. Genes with an absolute fold change greater than 2.5 are shown. SNORD3B-1, Homo sapiens small nucleolar RNA, C/D box 3B-1; EMILIN2, elastin microfibril interfacier 2; FABP4, fatty acid binding protein 4; MMP1, matrix metalloproteinase 1; ANO1, anoctamin 1; RELN, reelin; FPR2, formyl peptide receptor 2; UHMK1, U2AF homology motif kinase 1; RMND5A, required for meiotic nuclear division 5 homolog A; CAPZA1; capping protein (actin filament) muscle Z-line, alpha 1. *, $p < 0.05$; **, $p < 0.01$; ***, $p < 0.001$. (B) RT-QPCR confirmation of gene expression profiles after knockdown of AEG-1 in SAS and FaDu cells. All experiments were performed in triplicate ($n = 3$) and data were normalized to GAPDH. (C) secreted MMP1 protein in cell-conditioned culture media. Each cell lines were seeded in equal numbers (1×10^6 cells) and were cultured in starving condition (1% fetal bovine serum, FBS) for 24 hr and the media were harvested. (D) immunohistochemical staining of MMP1 in murine subcutaneous xenograft tumors (upper row) and metastatic lesions from *in vivo* lung metastasis assays (lower row). Scale bar: upper row, 100 μm ; lower row, 25 μm .

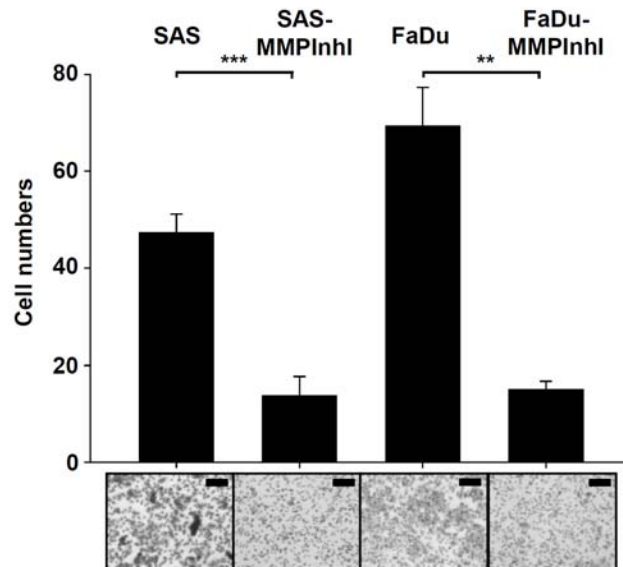


Figure 8. MMP inhibitor I (MMPInhI, 2 μ M) impede invasion of SAS and FaDu cells into Matrigel. All values are the average of three independent experiments. ***, $p < 0.001$; **, $p < 0.01$. Scale Bar: 130 μ m.

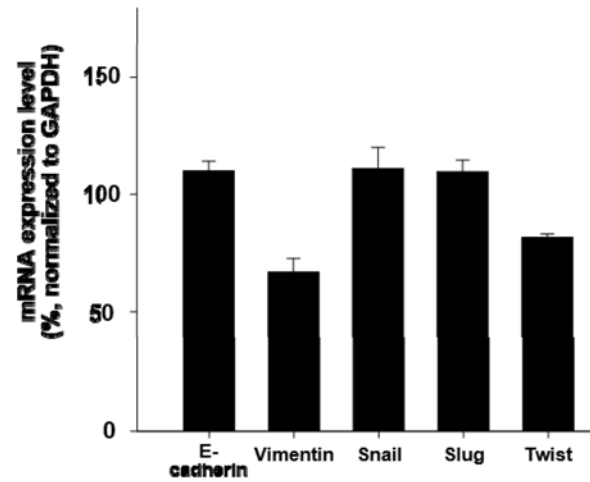


Figure 9. Alteration of expression profile of EMT-associated genes after knockdown of AEG-1 in SAS cells. QRT-PCR reveals down regulation of vimentin (67%) in SB cells when compared to SCt cells. Nevertheless, no significant fluctuation is noted in E-cadherin, Snail, and Slug.

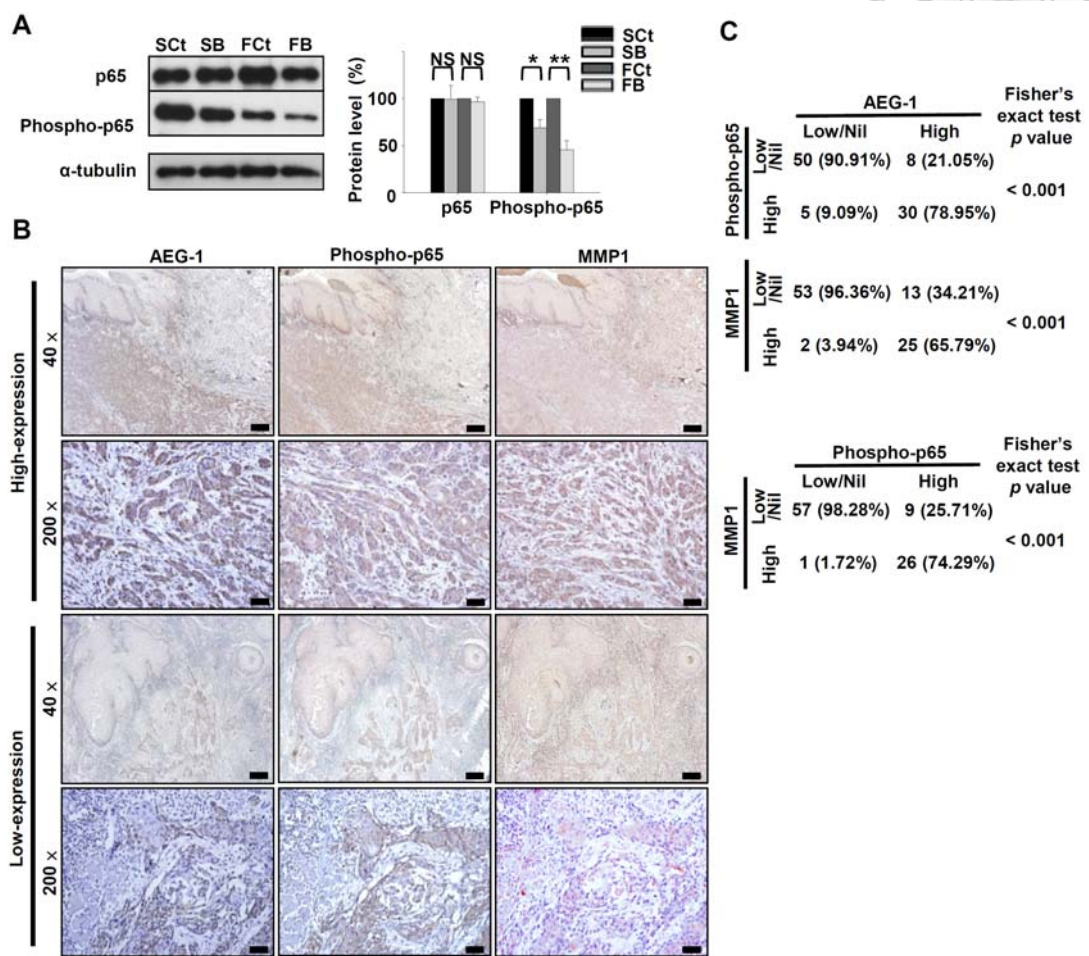


Figure 10. AEG-1 knockdown suppressed phosphorylation of serine 536 of the p65 subunit (RelA) of NF- κ B. (A) Western blot of total p65 and phosphorylated p65 (serine 536). Data were normalized to respective controls and are expressed as mean \pm SEM; $n = 3$. NS, not significant ($p > 0.05$); *, $p < 0.05$; **, $p < 0.01$. (B and C) immunohistochemical staining of phosphorylated p65 (Ser536) and MMP1 in formalin-fixed, paraffin embedded OSCC specimens. Expression of phosphorylated p65 and MMP1 was positively correlated with that of AEG-1 both intratumorally (B) and intertumourally (C). Scale bar: 40 \times , 300 μ m; 200 \times , 45 μ m.

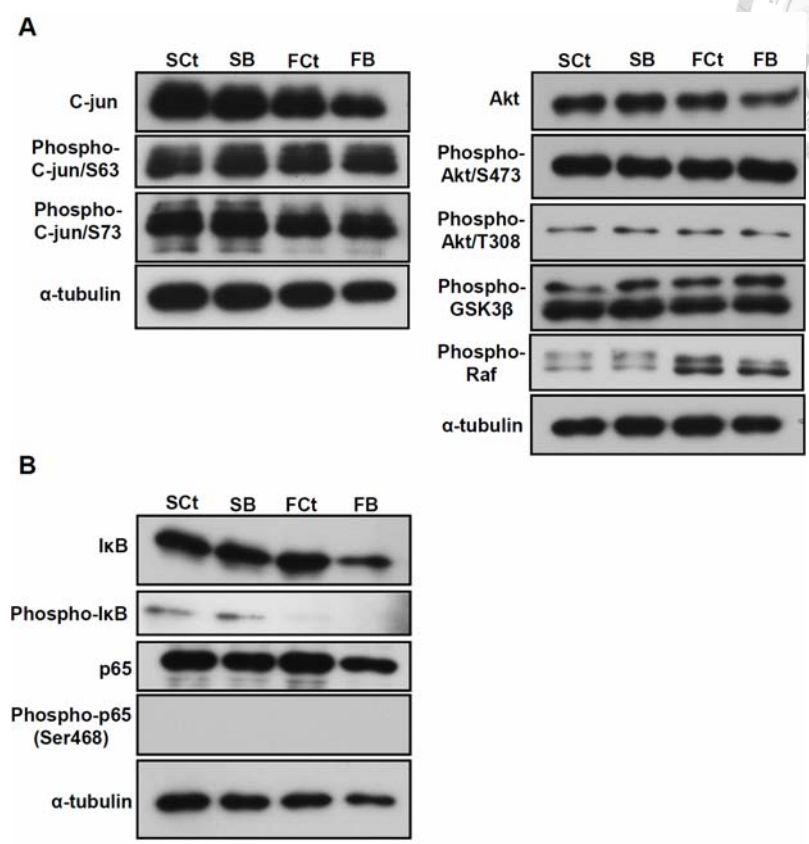
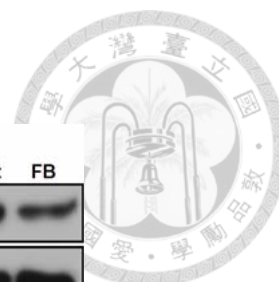


Figure 11. The phosphorylated status of components in PI3K pathway and NF κ B pathway. (A) C-jun and downstream effectors of PI3K pathway. (B) I κ B and p65 at amino acid residue serine 468.

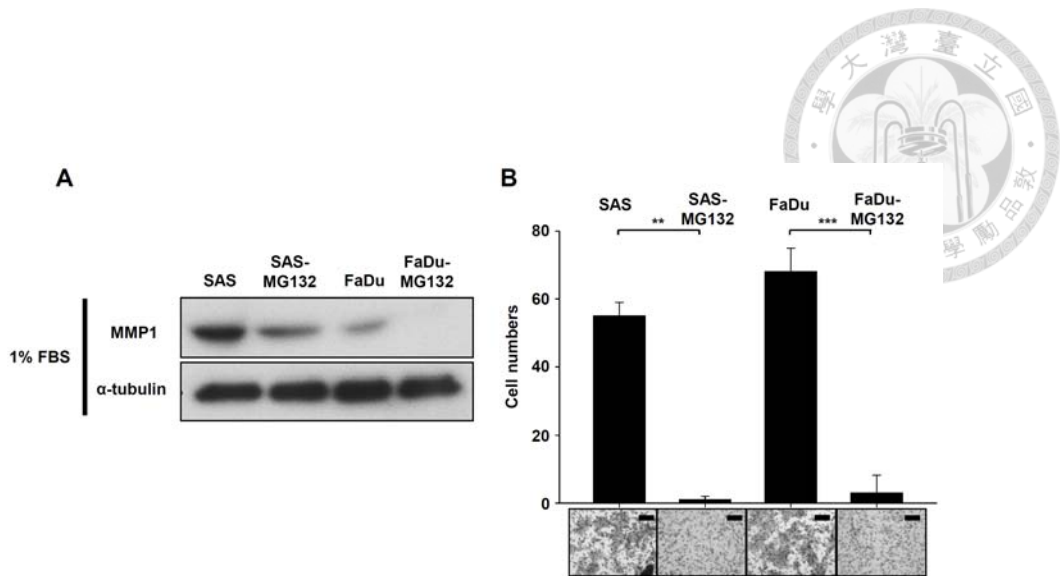


Figure 12. MG132, an inhibitor of NF- κ B, impede secretion of MMP1 and invasion of SAS and FaDu cells into Matrigel. (A) secreted MMP1 protein in cell-conditioned culture media. Each cell lines were seeded in equal numbers (1×10^6 cells) and were cultured in starving condition (1% FBS) with 5 μ M MG132 for 24 hr and the media were harvested. (B) Invasion assay with treatment of NF- κ B inhibitor. Cells were seeded into the coated hanging inserts (2×10^5 cells/insert) and incubated with the corresponding culture media with 5 μ M MG132. The lower chamber of the invasion system was filled with serum-free culture media. The cells and Matrigel on the upper side of the inserts were removed after 24 hr. All values are the average of three independent experiments. ***, $p < 0.001$; **, $p < 0.01$. Scale Bar: 130 μ m.

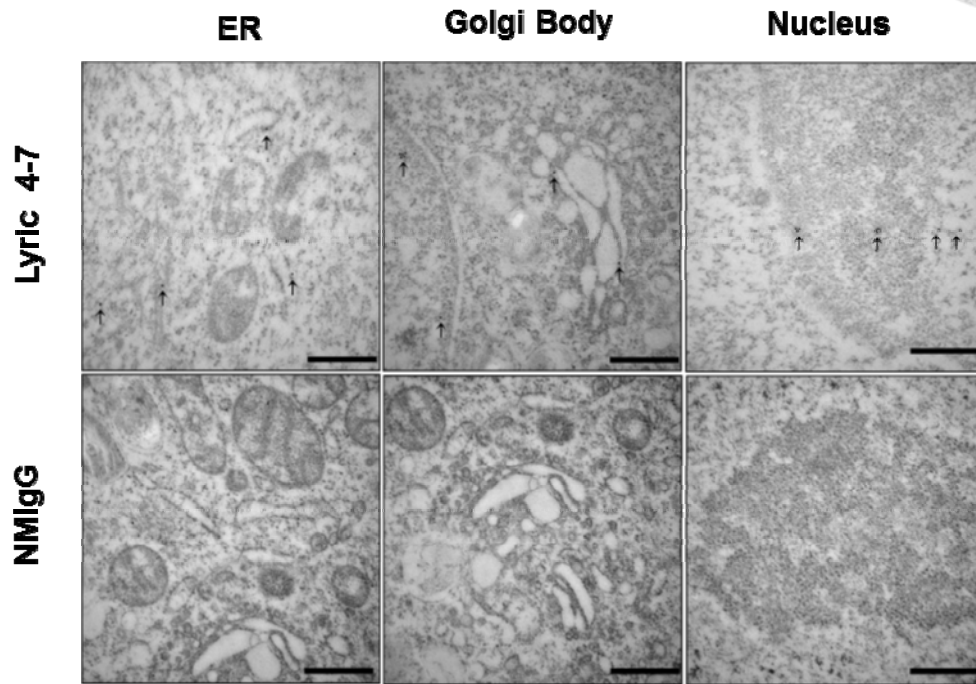


Figure 13. Localization of AEG-1 in SAS cells. After incubation with Lyric 4-7, an anti-murine IgG antibody conjugated with 18 nm gold particle was applied. Through transmission electromicroscope (TEM), a wide array of subcellular membranous compartments is positive for AEG-1, including ER, Golgi body as well as nucleus. Arrow: aggregates of gold particles. Scale bar: 500 nm.

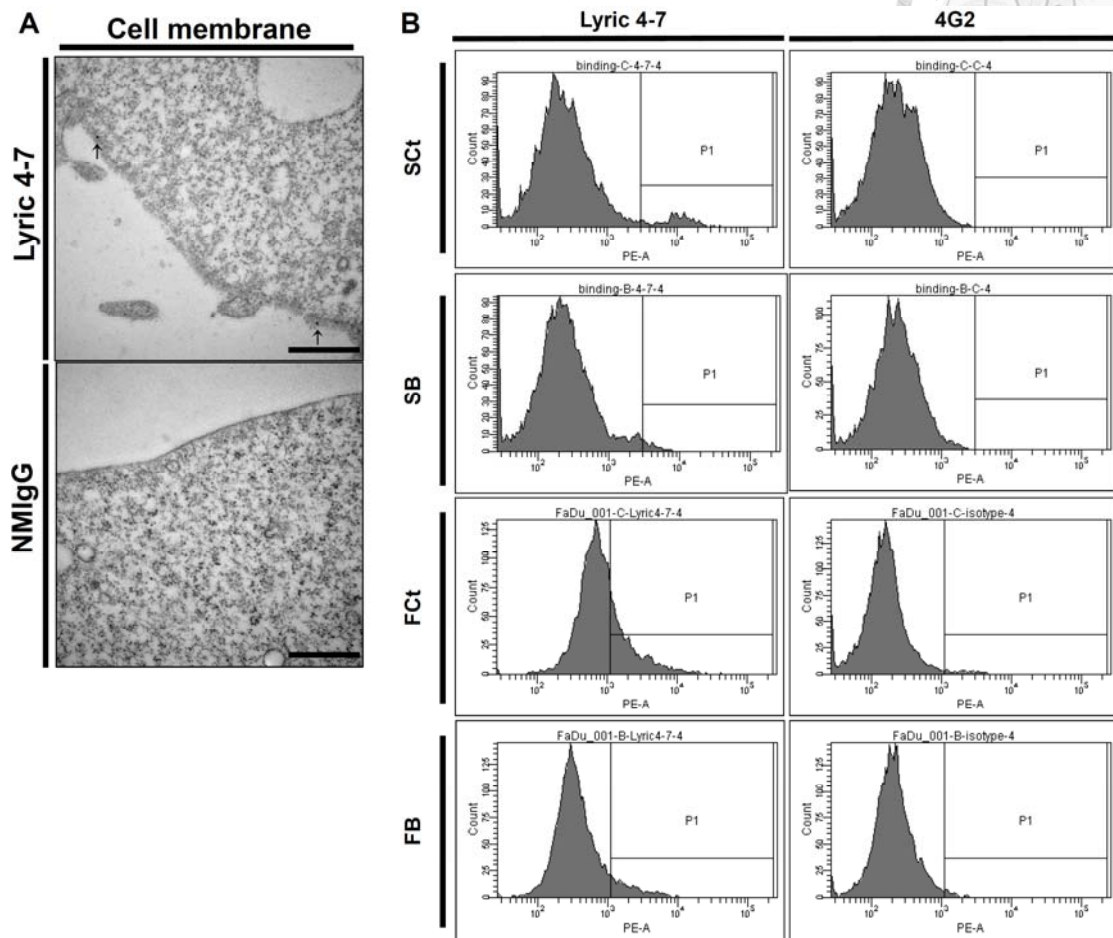


Figure 14. TEM observation. (A) gold particles (arrows) on the plasma membrane of SAS cells. Scale bar: 500 nm. (B) flow cytometry assay of membranous AEG-1 protein in HNSCC cell lines. A small population (5%) of high expression of membranous AEG-1 was found in SAS cells, whereas the FaDu cells exhibit a relatively higher baseline expression of membranous AEG-1 than SAS cells. Knockdown of AEG-1 with shRNA eliminated the high membranous AEG-1-expressed population in SAS cells and cause left-shift of the entire population in FaDu cells. Concentration of the antibodies, 0.37 $\mu\text{g/ml}$. 4G2, isotypic control antibody.

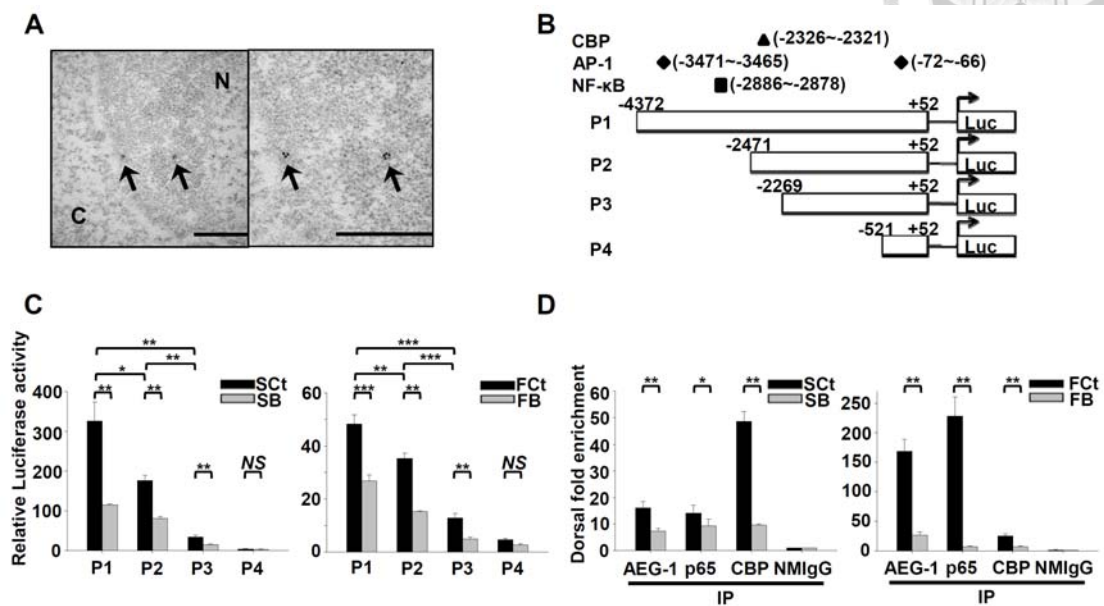


Figure 15. AEG-1 regulates MMP1 expression at the transcriptional level through enhancing the binding of p65 to MMP1 promoter. (A) nuclear translocation of AEG-1 protein was revealed by transmission electron microscopy. Arrow, 18 nm gold particles conjugated to anti-AEG-1 antibody. N, nucleus. C, cytosol. Right, magnified view. Scale bar, 500 nm. (B) constructs of the MMP1 promoter region used for the luciferase reporter assay. (C) transactivating activity of AEG-1 on MMP1 promoter constructs in the SAS and FaDu cell lines. All data were expressed as mean \pm SEM; n = 3. (D) ChIP assay showing AEG-1, p65 and CBP binding to the NF- κ B binding site of the MMP1 promoter in SAS and FaDu cell lines. NMIgG served as a negative control. All data were expressed as mean \pm SEM; n = 3. NS, not significant ($p > 0.05$); *, $p < 0.05$; **, $p < 0.01$; ***, $p < 0.001$.

Tables



Table 1

Clinicopathological correlation with AEG-1 in 93 cases of OSCC

Parameter	AEG-1 expression status		Fisher's exact test p value
	Low No. (%)	High No. (%)	
Gender			
Male	46 (83.64%)	33 (86.84%)	0.773
Female	9 (16.36%)	5 (13.16%)	
Age			
>50 y/o	36 (65.45%)	20 (52.63%)	0.282
<50 y/o	19 (34.55%)	18 (47.37%)	
Location			
Buccal mucosa	22 (40.00%)	18 (47.37%)	0.307
Gingiva	11 (20.00%)	3 (7.89%)	
Floor of the mouth	1 (1.81%)	2 (5.26%)	
Lip	0 (0%)	2 (5.26%)	
Tongue	19 (34.55%)	12 (31.58%)	
Palate	2 (3.64%)	1 (2.64%)	
Stage			
I+II	30 (54.55%)	10 (26.32%)	0.01
III+IV	25 (45.45%)	28 (73.68%)	
T			
T1+T2	31 (56.36%)	22 (57.89%)	1.000
T3+T4	24 (43.64%)	16 (42.11%)	
N			
N0	47 (85.45%)	17 (44.74%)	<0.001
N1+N2+N3	8 (14.55%)	21 (55.26%)	
M			
M0	54 (98.18%)	34 (89.47%)	0.155
M1	1 (1.82%)	4 (10.53%)	
Recurrence			
Negative	45 (81.82%)	30 (78.95%)	0.793
Positive	10 (18.18%)	8 (21.05%)	
Differentiation			
Well	48 (87.27%)	27 (71.05%)	0.064
Moderate/poor	7 (12.73%)	11 (28.95%)	
Alcohol			
Negative	24 (43.64%)	10 (26.32%)	0.125
Positive	31 (56.36%)	28 (73.68%)	
Betel nut			
Negative	16 (29.09%)	6 (15.79%)	0.214
Positive	39 (70.91%)	32 (84.21%)	
Cigarette			
Negative	14 (25.45%)	8 (21.05%)	0.805
Positive	41 (74.55%)	30 (78.95%)	



Table 2

**Correlation of advanced lymph node metastasis with AEG-1
in 93 cases of OSCC**

Parameter	AEG-1 expression status		Fisher's exact test <i>p</i> value
	Low No. (%)	High No. (%)	
N			
N0+N1	50 (90.91%)	26 (68.42%)	0.012
N2+N3	5 (9.09%)	12 (31.58%)	



Table 3

**Clinicopathological correlation with phosphorylated p65
(serine 536) in 93 cases of OSCC**

Parameter	pP65 expression status		Fisher's exact test p value
	Low No. (%)	High No. (%)	
Stage			
I+II	32 (55.17%)	8 (22.86%)	0.003
III+IV	26 (44.83%)	27 (77.14%)	
T			
T1+T2	34 (58.62%)	19 (54.29%)	0.829
T3+T4	24 (41.38%)	16 (45.71%)	
N			
N0	50 (86.21%)	14 (40.00%)	<0.001
N1+N2+N3	8 (13.79%)	21 (60.00%)	
M			
M0	57 (98.28%)	31 (88.57%)	0.065
M1	1 (1.72%)	4 (11.43%)	
Recurrence			
Negative	47 (81.03%)	28 (80.00%)	1.000
Positive	11 (18.97%)	7 (20.00%)	
Differentiation			
Well	51 (87.93%)	24 (68.57%)	0.03
Moderate/poor	7 (12.07%)	11 (31.43%)	



Table 4

Clinicopathological correlation with MMP1 in 93 cases of OSCC

Parameter	MMP1 expression status		Fisher's exact test <i>p</i> value
	Low No. (%)	High No. (%)	
Stage			
I+II	36 (54.55%)	4 (14.81%)	<0.001
III+IV	30 (45.45%)	23 (85.19%)	
T			
T1+T2	40 (60.61%)	13 (48.15%)	0.357
T3+T4	26 (39.39%)	14 (51.85%)	
N			
N0	55 (83.33%)	9 (33.33%)	<0.001
N1+N2+N3	11 (16.67%)	18 (66.67%)	
M			
M0	65 (98.48%)	23 (85.19%)	0.024
M1	1 (1.52%)	4 (14.81%)	
Recurrence			
Negative	60 (90.91%)	22 (81.48%)	0.287
Positive	6 (9.09%)	5 (18.52%)	
Differentiation			
Well	57 (86.36%)	18 (66.67%)	0.042
Moderate/poor	9 (13.94%)	9 (33.33%)	

Appendix



Curriculum Vita



Name: Yi-Ping, Wang

Date of Birth: May 30, 1978

Gender: Male

Mailing Address: No.1, Changde St., Zhongzheng Dist., Taipei City 10048, Taiwan

Telephone: +886-2-2312-3456 #67987

FAX: Nil

E-mail: ypwang0530@ntu.edu.tw

Education:

National Taiwan University, Taipei, Taiwan M.S. 2004 Oral Pathology

National Taiwan University, Taipei, Taiwan D.D.S. 2002 Dentistry

Employment

2009-present Attending Staff, Division of Oral Diagnosis, Department of Dentistry,
National Taiwan University Hospital, Taipei, Taiwan

Instructor, Faculty of Dentistry, School of Dentistry, National Taiwan,
University, Taipei, Taiwan

2008-2009 Adjunct Attending Staff, Division of Oral Diagnosis, Department of
Dentistry, National Taiwan University Hospital, Taipei, Taiwan

2004-2008 Resident, Department of Dentistry, National Taiwan University
Hospital, Taipei, Taiwan

Board Certification:

2007-present Diplomat, Taiwan Academy of Oral Pathology, Taiwan